the ER Ca^{2+}-ATPase inhibitors (21) thapsigargin and cyclopiazonic acid, the ryanodine receptor activator 4-chloro-*m*-cresol, and the protein *N*-glycosylation inhibitor tunicamycin all induced WFS1 protein as shown in Fig. 3. Only brefeldin A had no effect. Ionomycin only weakly induced WFS1 protein. The differing effects of these chemicals, which have different mechanisms of action, may provide insights into the functions of Wfs1. The lack of WFS1 induction with brefeldin A, a Golgi apparatus disruptor, may be related to its instability in solution (22). Although we did not perform Northern blot analysis for each of these reagents, A23187 induced *WFS1* mRNA in fibroblasts (data not shown).

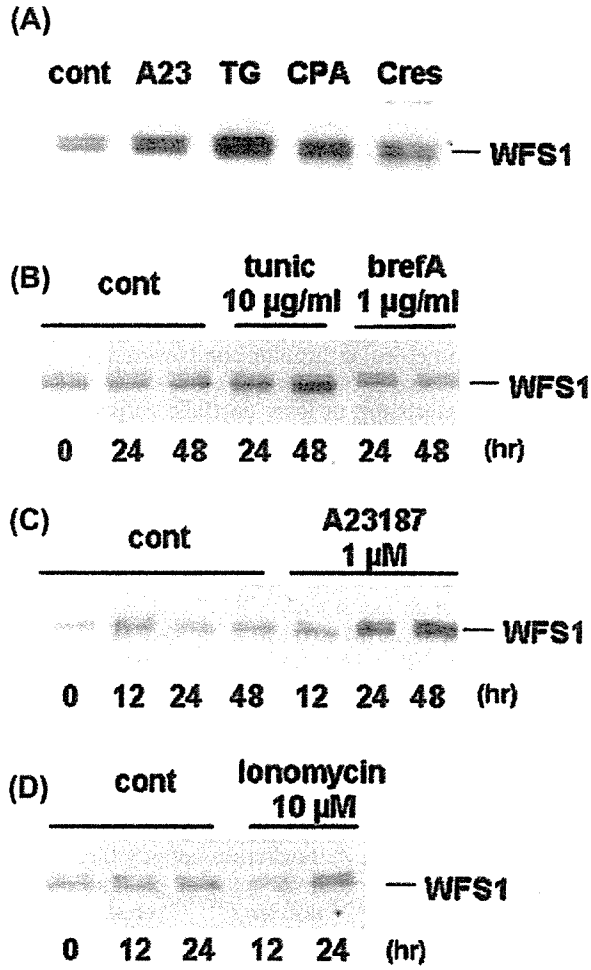

Figure 3 ER stress induces WFS1 protein in fibroblasts. Primary skin fibroblasts were cultured in the presence of (A) A23187 (A23, 1 μmol/l), thapsigargin (TG, 1 μmol/l), cyclopiazonic acid (CPA, 10 μmol/l) and 4-chloro-*m*-cresol (cres, 50 μmol/l) for 48 h. (B–D) Cells were treated for the indicated time periods with (B) tunicamycin (tunic), brefeldin A (brefA), (C) A23187, and (D) ionomycin. cont indicates control. Control samples included a vehicle (DMSO), also administered with all of the drugs. Cells were harvested after the incubation periods, and total cell lysates containing 20 μg protein were subjected to Western blot analysis using anti-WFS1c antibody.

Effects of thapsigargin and tunicamycin on Wfs1 *expression in MIN6 cells*

We next examined the effects of thapsigargin and tunicamycin on the expression of *Wfs1* mRNA in MIN6 cells. Thapsigargin and tunicamycin treatments are known to induce ER stress, and Chop/GADD153 is a transcription factor that plays a role in ER stress-induced apoptotic cell death (23, 24). Phosphorylation of the α-subunit of translation initiation factor-2 (eIF2-α) attenuates protein translation upon ER stress. Although the ER chaperone Bip/GRP78 expression did not change in MIN6 cells (Fig. 4B) probably due to its strong basal expression, thapsigargin and tunicamycin clearly generated ER stress as demonstrated by Chop induction and eIF2-α phosphorylation (Fig. 4A, B). Under these conditions, ER stress-induced caspase-3 activation, an event at the initiation of apoptosis (25), was evidenced by the cleavage of PARP (Fig. 4C). PARP is one of the substrates cleaved by caspase-3. Upon thapsigargin or tunicamycin treatment, the 113 kDa band decreased, and instead, the proteolytic PARP fragment (89 kDa) appeared (Fig. 4C). In association with ER stress induction and caspase-3 activation, *Wfs1* mRNA expression increased (Fig. 4A,D). With thapsigargin, *Wfs1* mRNA started to increase after 6 h and was maximal after 12 h. With tunicamycin, *Wfs1* mRNA induction peaked at 6 h, and then declined. Wfs1 protein was also increased by thapsigargin treatment (Fig. 4B). In contrast, tunicamycin, despite the mRNA induction, did not increase the Wfs1 protein, but decreased it after 24 h (Fig. 4B). This is probably due to the instability of unglycosylated Wfs1 protein (6, 16).

Thapsigargin and tunicamycin enhance human WFS1 *promoter activity in MIN6 cells*

To determine the mechanism of *WFS1* expression, we examined the effects of thapsigargin and tunicamycin on human *WFS1* gene promoter activity by employing transient transfection assays in MIN6 cells. We used a *WFS1* promoter-luciferase construct that contained a 3 kb DNA sequence upstream from the human *WFS1* gene transcription initiation site. The human *WFS1* gene promoter was active in MIN6 cells. Introduction of the *WFS1* promoter-reporter plasmid produced a 20-fold increase in luciferase activity as compared with the promoterless pGL3-Basic vector. Treatment of the cells with thapsigargin or tunicamycin resulted in further 1.3- and 1.5-fold increases in luciferase activity respectively (Fig. 5). We conducted these experiments again using a 1 kb (−1000 to +20) *WFS1* promoter-luciferase reporter gene. The results were essentially the same but the promoter activity was weaker than with the 3 kb construct (data not shown).

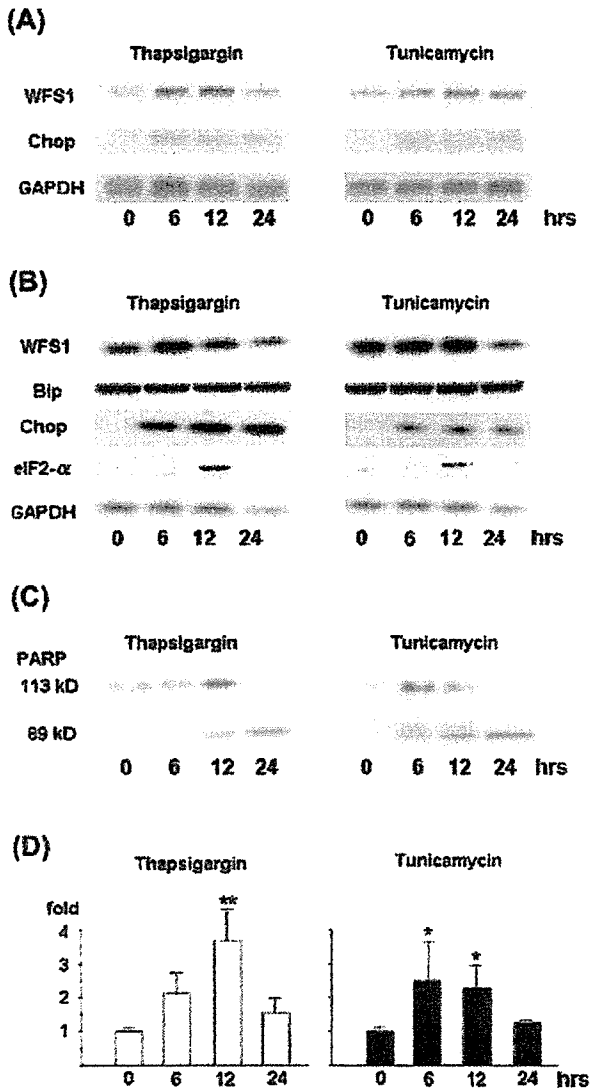

Figure 4 Thapsigargin and tunicamycin increase *Wfs1* mRNA expression in MIN6 cells in association with ER stress and apoptosis induction. MIN6 cells were placed in culture dishes and serum-starved in serum-free DMEM for 12 h, and then treated with thapsigargin (1 μmol/l) or tunicamycin (10 μg/ml) for 6, 12 or 24 h. Dimethyl sulfoxide (DMSO) was used to dissolve thapsigargin and tunicamycin, and the same concentration of DMSO (final, 0.05%) was employed in all experiments, including controls. After incubation, cells were washed once with ice-cold phosphate-buffered saline, and harvested. (A) Ten micrograms RNA were subjected to Northern blot analysis. (B) Total cell lysates containing equal amounts of protein (50 μg) were separated on 10% SDS-PAGE and analyzed by immunoblotting using anti-Wfs1n, anti-Bip (GRP74), anti-Chop or anti-phosphorylated eIF2-α, (C) Total cell lysates containing equal amounts of protein (50 μg) were separated on 10% SDS-PAGE and analyzed by immunoblotting using the anti-PARP antibody. Activated caspase-3 cleaves the 113 kDa PARP, resulting in the appearance of the 89 kDa fragment. (D) Quantification of the *Wfs1* mRNA from the results obtained in (A), shown as means±S.E. ($n = 4$). Statistical analysis, conducted using analysis of variance, indicated that the thapsigargin and tunicamycin treatments significantly increased *Wfs1* mRNA expression at 12 h and at 6 h and 12 h respectively (*$P < 0.05$, **$P < 0.001$).

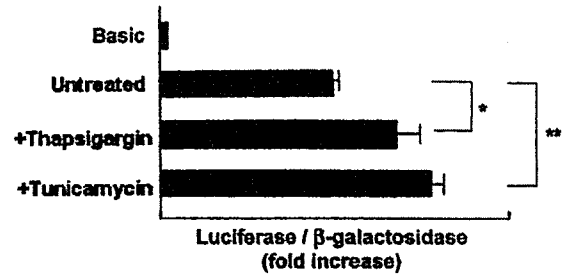

Figure 5 ER stress enhances *WFS1* promoter activity in MIN6 cells. MIN6 cells were transfected with a luciferase reporter plasmid containing a 3.0 kb human *WFS1* gene 5' flanking promoter region (from −3000 to +20) and were exposed to thapsigargin (1 μmol/l) or tunicamycin (10 μg/ml) for 6 h. Beta-galactosidase activity from the co-transfected expression vector pCMVβ was used to calibrate for transfection efficiency. Basic represents luciferase activity from pGL3-Basic (promoterless) vector-transfected cells. Results are expressed as the fold increase as compared with basic (means±S.E. of four independent experiments, each performed in triplicate). *P* values for comparison of results with versus without drug treatments are 0.034 (thapsigargin, *) and 0.005 (tunicamycin, **) (analysis of variance).

Wfs1 *expression is transcriptionally upregulated in β-cells with intrinsic ER stress*

In the Akita mouse, the C96Y mutation of the *ins2* gene disturbs intramolecular disulfide bond formation, resulting in progressive β-cell loss (12). ER stress and subsequent apoptosis are at least partially responsible for this progressive β-cell loss (14). To further examine the association between increased *Wfs1* expression and ER stress, we used mouse insulinoma cells derived from an Akita mouse homozygous for the *ins2* gene C96Y mutation (*Ins2* $^{96Y/Y}$ cell) as a model. *Ins2* $^{WT/WT}$ cells derived from normal littermates served as controls. Doubling of the ER chaperone Bip/GRP78 in *Ins2* $^{96Y/Y}$ cells indicated persistent ER stress in these cells (Fig. 6A). In Ins2$^{96Y/Y}$ cells, Wfs1 protein increased sixfold as compared with that in *Ins2* $^{WT/WT}$ cells (Fig. 6B). *Wfs1* mRNA expression was also increased twofold (data not shown). We next examined *WFS1* promoter activity in these cells. Introduction of the *WFS1* promoter-reporter plasmid into *Ins2* $^{96Y/Y}$ cells approximately doubled luciferase activity as compared with that in wild type *Ins2* $^{WT/WT}$ cells (Fig. 7). Luciferase activity after transfection of the SV40 promoter-reporter plasmid did not differ between *Ins2* $^{96Y/Y}$ and *Ins2* $^{WT/WT}$ cells.

Discussion

Herein, we have documented the localization of Wfs1 expression in the mouse pancreatic islet. Insulin-producing β-cells are the major site of Wfs1 expression, as shown in Ishihara *et al.* (15). Wfs1 expression is also evident in somatostatin-producing δ-cells, but is absent from glucagon producing α-cells and PP-cells. No *Wfs1* expression is observed in pancreatic exocrine acinar

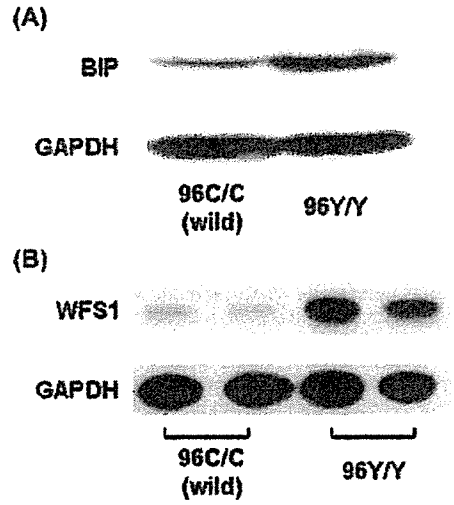

Figure 6 *WFS1* expression is increased in Akita mouse-derived *Ins2*$^{96Y/Y}$ cells. Cell extracts of *Ins2*$^{96Y/Y}$ cells containing equal amounts of protein (50 μg) were separated on 10% SDS-PAGE and analyzed by immunoblotting using (A) anti-Bip, and (B) anti-WFS1n and anti-GAPDH antibodies. Insulinoma cells derived from wild type littermates (wild) were used as the control. In (B), cell extracts were prepared on two separate occasions from cells derived from the same mutant mouse.

cells. A histopathological study of pancreatic islets from Wolfram syndrome patients showed selective loss of insulin-producing β-cells and an apparent preservation of glucagon-producing α-, somatostatin-producing δ-, and PP-cells (26, 27). The histochemical evidence of Wfs1 protein localization in insulin-producing β-cells might provide a histological background explaining the insulin deficiency caused by *WFS1* mutations in Wolfram syndrome patients and suggests that WFS1 protein is necessary for β-cell (28, 29), but not δ-cell survival.

We have also presented evidence herein that ER stress induces *Wfs1* gene expression. Treatment of fibroblasts with A23187, ionomycin, thapsigargin, cyclopiazonic acid, 4-chloro-*m*-cresol or tunicamycin increased *Wfs1* protein levels. Chemical insults by these reagents are known to induce ER stress via disruption of Ca^{2+} homeostasis or inhibition of N-linked glycosylation. Thapsigargin and tunicamycin treatments also induced *Wfs1* mRNA expression in a mouse β-cell line, MIN6 cells. In accordance with the mRNA change, thapsigargin increased Wfs1 protein expression. However, the Wfs1 protein level in MIN6 cells did not change with tunicamycin. This is probably due to Wfs1 being an N-glycosylated protein, and inhibition of glycosylation by tunicamycin decreases its stability (6, 16). Increased *Wfs1* expression in association with ER stress was further demonstrated in another β-cell model with ER stress: *Ins2*$^{96Y/Y}$ cells derived from the Akita mouse. The Akita mouse spontaneously develops early-onset non-obese diabetes with a reduced β-cell mass, which is caused by a conformation-altering missense mutation (Cys96Tyr) in the insulin-2 gene (12, 13). Intramolecular disulfide-bond formation is disrupted in the mutant insulin molecule. It was reported that this misfolded mutant insulin expression constitutively induced ER stress in Akita mouse β-cells (14). We have indeed confirmed increased Bip protein expression in *Ins2*$^{96Y/Y}$ cells as compared with wild type *Ins*$^{WT/WT}$ cells derived from normal littermates. In *Ins2*$^{96Y/Y}$ cells, *Wfs1* mRNA (data not shown) and protein levels (Fig. 6) were both increased. The increased *Wfs1* mRNA (twofold, data not shown) was consistent with the increased *Wfs1* promoter activity (Fig. 7). Our results provide further evidence, i.e. a detailed analysis, that *Wfs1* expression increases in association with ER stress, especially in the pancreatic β-cells selectively lost in patients with Wolfram syndrome. It is noteworthy that the increase in Wfs1 protein was marked (sixfold) as compared with the modest increase in Bip expression (twofold) in *Ins2*$^{96Y/Y}$ cells. Mechanisms other than ER stress might have further increased Wfs1 protein expression in this cell line.

The increase in *Wfs1* expression is attributable, at least in part, to enhanced *Wfs1* transcription, because both ER stress-inducing chemical insults (MIN6 cells) and intrinsic ER stress (*Ins2*$^{96Y/Y}$cells) stimulated *WFS1* promoter activity as demonstrated by a transient transfection assay using a human *WFS1* promoter-luciferase reporter construct. A cis-acting ER stress responsive element (ERSE) has been identified in the proximal promoter regions of chaperone-encoding genes. This element consists of a consensus sequence of

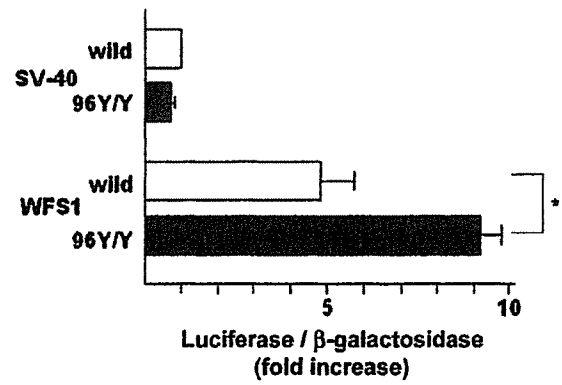

Figure 7 *WFS1* promoter activity is enhanced in *Ins2*$^{96Y/Y}$ cells. *Ins2*$^{96Y/Y}$ cells or wild type (wild) control cells were transfected with a luciferase reporter plasmid containing the 3.0 kb human *WFS1* gene 5′ flanking promoter region (from −3000 to +20), or a control plasmid containing the SV40 promoter-luciferase reporter. The expression vector pCMVβ was co-transfected, and β-galactosidase activity was used to calibrate for transfection efficiency. Results are expressed as fold-increases relative to luciferase/β-galactosidase activities in *Ins2*$^{96Y/Y}$cells as compared with control *Ins2*$^{WT/WT}$ cells in four independent experiments (means±S.E.), each performed in triplicate. *WFS1* promoter activity was significantly increased in *Ins2*$^{96Y/Y}$ cells as compared with control *Ins2*$^{WT/WT}$ cells (*$P = 0.014$, Student's *t*-tests).

CCAAT-N9-CCACG (30). The general transcriptional factor, NF-Y/CBF, binds to the CCAAT motif of the ERSE (31). Once ER stress ensues, p50ATF6 (active form of transcriptional factor ATF6) binds to the CCACG motif of the ERSE (31, 32) resulting in transcriptional induction of ER chaperones. Another ERSE (ERSE-II) with a consensus sequence of ATTGG-N-CCACG has also been identified (32). Although there are six CCAAT motifs in the −2800 to −2300 region of the putative human *WFS1* promoter, we found no ERSE consensus sequences within 3 kb upstream from the transcription initiation site. Further studies will be required to elucidate the mechanism of transcriptional regulation of the *Wfs1* gene via ER stress.

The observations made in this study suggest that Wfs1 protein may be involved in the ER stress response pathway, i.e. the unfolded protein response, in which cells respond by inducing chaperones, attenuating protein translation, and inducing apoptosis. Pancreatic β-cells suffer under chronic ER stress, striving to meet the increasing demands of insulin biosynthesis and secretion. In patients with Wolfram syndrome (26) and in *Wfs1* knock-out mice (15), β-cells were selectively lost from pancreatic islets. Moreover, islets from *Wfs* $^{-/-}$ mice were highly susceptible to ER stress (thapsigargin and tunicamycin)-induced apoptosis (15). It is tempting to speculate that Wfs1 protein is upregulated in response to ER stress and that it plays a physiological role in protecting cells from ER stress-induced apoptosis. Loss of function mutations of the *Wfs1* gene may cause β-cell loss due to disruption of this protective function. It was recently reported that Wfs1 protein expressed in oocytes exhibited a cation-selective ion channel activity (7). Expression of Wfs1 protein in oocytes increased cytosolic Ca^{2+} levels (7), and islets from *Wfs1* $^{-/-}$ mice exhibited attenuated glucose-stimulated intracellular Ca^{2+} responses (15). Wfs1 protein may be involved in the maintenance of ER and intracellular Ca^{2+} homeostasis, and its expression is induced under conditions of perturbed homeostasis, including ER stress.

The current findings that Wfs1 protein, which is predominantly expressed in pancreatic islet β-cells, is transcriptionally upregulated by ER stress indicate a link between Wfs1 protein function and ER stress responses. Further investigations utilizing *Wfs1* $^{-/-}$ mice and *Wfs1* $^{-/-}$ β-cells will provide insights into Wfs1 protein function and the pathophysiology of Wolfram syndrome.

Acknowledgements

We thank Professor Junichi Miyazaki, Osaka University, Japan, for providing us with MIN6 cells. This study was supported in part by Grants-in-Aid for Scientific Research (14370338 and 16390096 to Y Tanizawa) from the Ministry of Education, Culture, Sports, Science and Technology of Japan, grant no.15591228 (to J Kawano) from the Japan Society for Promotion of Science, and a grant from Takeda Science Foundation.

References

1 Barrett TG & Bundey SE. Wolfram (DIDMOAD) syndrome. *Journal of Medical Genetics* 1997 **34** 838–841.
2 Barrett TG, Bundey SE & Macleod AF. Neurodegeneration and diabetes: UK nationwide study of Wolfram (DIDMOAD) syndrome. *Lancet* 1995 **346** 1458–1463.
3 Inoue H, Tanizawa Y, Wasson J, Behn P, Kalidas K, Bernal-Mizrachi E, Mueckler M, Marshall H, Donis-Keller H, Crock P, Rogers D, Mihuni M, Kumashiro H, Higashi K, Sobue G, Oka Y & Permutt MA. A gene encoding a transmembrane protein is mutated in patients with diabetes mellitus and optic atrophy (Wolfram syndrome). *Nature Genetics* 1998 **20** 143–148.
4 Strom TM, Hortnagel K, Hofmann S, Gekeler F, Scharfe C, Rabl W, Gerbitz KD & Meitinger T. Diabetes insipidus, diabetes mellitus, optic atrophy and deafness (DIDMOAD) caused by mutations in a novel gene (wolframin) coding for a predicted transmembrane protein. *Human Molecular Genetics* 1998 **7** 2021–2028.
5 Takeda K, Inoue H, Tanizawa Y, Matsuzaki Y, Oba J, Watanabe Y, Shinoda K & Oka Y. WFS1 (Wolfram syndrome 1) gene product: predominant subcellular localization to endoplasmic reticulum in cultured cells and neuronal expression in rat brain. *Human Molecular Genetics* 2001 **10** 477–484.
6 Hofmann S, Philbrook C, Gerbitz K-D & Bauer MF. Wolfram syndrome: structural and functional analyses of mutant and wild-type wolframin, the WFS1 gene product. *Human Molecular Genetics* 2003 **12** 2003–2012.
7 Osman AA, Saito M, Makepeace C, Permutt MA, Schlesinger P & Mueckler M. Wolframin expression induces novel ion channel activity in endoplasmic reticulum membranes and increases intracellular calcium. *Journal of Biological Chemistry* 2003 **26** 52755–52762.
8 Chevet E, Cameron PH, Pelletier MF, Thomas DY & Bergeron JJ. The endoplasmic reticulum: integration of protein folding, quality control, signaling and degradation. *Current Opinion in Structural Biology* 2001 **11** 120–124.
9 Rutkowski DT & Kaufman RJ. A trip to the ER: coping with stress. *Trends in Cell Biology* 2004 **14** 20–28.
10 Oyadomari S, Araki E & Mori M. Endoplasmic reticulum stress-mediated apoptosis in pancreatic β-cells. *Apoptosis* 2002 **7** 335–345.
11 Ron D. Proteotoxicity in the endoplasmic reticulum: lessons from the Akita diabetic mouse. *Journal of Clinical Investigation* 2002 **109** 443–445.
12 Yoshioka M, Kayo T, Ikeda T & Koizumi A. A novel locus, Mody 4, distal to D7Mit189 on chromosome 7 determines early-onset NIDDM in nonobese C57BL/6 (Akita) mutant mice. *Diabetes* 1997 **46** 887–894.
13 Wang J, Takeuchi T, Tanaka S, Kubo SK, Kayo T, Lu D, Takata K, Koizumi A & Izumi T. A mutation in the insulin 2 gene induces diabetes with severe pancreatic β-cell dysfunction in the Mody mouse. *Journal of Clinical Investigation* 1999 **103** 27–37.
14 Oyadomari S, Koizumi A, Takeda K, Gotoh T, Akira S, Araki E & Mori M. Targeted disruption of the Chop gene delays endoplasmic reticulum stress–mediated diabetes. *Journal of Clinical Investigation* 2002 **109** 525–532.
15 Ishihara H, Takeda S, Tamura A, Takahashi R, Yamaguchi S, Takei D, Yamada T, Inoue H, Soga H, Katagiri H, Tanizawa Y & Oka Y. Disruption of the WFS1 gene in mice causes progressive β-cell loss and impaired stimulus-secretion coupling in insulin secretion. *Human Molecular Genetics* 2004 **13** 1159–1170.
16 Yamaguchi S, Ishihara H, Tamura A, Yamada T, Takahashi R, Takei D, Katagiri H & Oka Y. Endoplasmic reticulum stress and

N-glycosylation modulate expression of WFS1 protein. *Biochemical and Biophysical Research Communication* 2004 **3** 250–256.
17 Nozaki J, Kubota H, Yoshida H, Naitoh M, Goji J, Yoshinaga T, Mori K, Koizumi A & Nagata K. The endoplasmic reticulum stress response is stimulated through the continuous activation of transcription factors ATF6 and XBP1 in Ins2 + /Akita pancreatic beta cells. *Genes to Cells* 2004 **9** 261–270.
18 Sheng Z, Kawano J, Yanai A, Fujinaga R, Tanaka M, Watanabe Y & Shinoda K. Expression of estrogen receptors (α,β) and androgen receptor in serotonin neurons of the rat and mouse dorsal raphe nuclei; sex and species differences. *Neuroscience Research* 2004 **49** 185–196.
19 Miyazaki J, Araki K, Yamato E, Ikegami H, Asano T, Shibasaki Y, Oka Y & Yamamura K. Establishment of a pancreatic beta cell line that retains glucose-inducible insulin secretion: special reference to expression of glucose transporter isoforms. *Endocrinology* 1990 **127** 126–132.
20 Oka Y, Asano T, Shibasaki Y, Kasuga M, Kanazawa Y & Takaku F. Studies with antipeptide antibody suggest the presence of at least two types of glucose transporter in rat brain and adipocyte. *Journal of Biological Chemistry* 1988 **263** 13432–13439.
21 Li WW, Alexandre S, Cao X & Lee AS. Transactivation of the grp78 promoter by Ca^{2+} depletion. A comparative analysis with A23187 and the endoplasmic reticulum $Ca^{(2+)}$-ATPase inhibitor thapsigargin. *Journal of Biological Chemistry* 1993 **268** 12003–12009.
22 Fujiwara T, Oda K, Yokota S, Takatsuki A & Ikehara Y. Brefeldin A causes disassembly of the Golgi complex and accumulation of secretory proteins in the endoplasmic reticulum. *Journal of Biological Chemistry* 1988 **263** 18545–18552.
23 Zinszner H, Kuroda M, Wang X, Batchvarova N, Lightfoot RT, Remotti H, Stevens JL & Ron D. CHOP is implicated in programmed cell death in response to impaired function of the endoplasmic reticulum. *Genes and Development* 1998 **12** 982–995.
24 McCullough KD, Martindale JL, Klotz LO, Aw TY & Holbrook NJ. Gadd153 sensitizes cells to endoplasmic reticulum stress by downregulating Bcl2 and perturbing the cellular redox state. *Molecular and Cellular Biology* 2001 **21** 1249–1259.
25 Nicholson DW, Ali A, Thornberry NA, Vaillancourt JP, Ding CK, Gallant M, Gareau Y, Griffin PR, Labelle M & Lazebnik YA. Identification and inhibition of the ICE/CED-3 protease necessary for mammalian apoptosis. *Nature* 1995 **376** 37–43.
26 Karasik A, O'Hara C, Srikanta S, Swift M, Soeldner JS, Kahn CR & Herskowitz RD. Genetically programmed selective islet beta-cell loss in diabetic subjects with Wolfram's syndrome. *Diabetes Care* 1989 **12** 135–138.
27 Kinsley BT, Swift M, Dumont RH & Swift RG. Morbidity and mortality in the Wolfram syndrome. *Diabetes Care* 1995 **18** 1566–1570.
28 Gerbitz K-D. Reflexions on a newly discovered diabetogenic gene, wolframin (WFS1). *Diabetologia* 1999 **42** 627–630.
29 Minton JA, Rainbow LA, Ricketts C & Barrett TG. Wolfram syndrome. *Reviews in Endocrine and Metabolic Disorders* 2003 **4** 53–59.
30 Yoshida H, Haze K, Yanagi H, Yura T & Mori K. Identification of the cis-acting endoplasmic reticulum stress response element responsible for transcriptional induction of mammalian glucose-regulated proteins. Involvement of basic leucine zipper transcription factors. *Journal of Biological Chemistry* 1998 **273** 33741–33749.
31 Yoshida H, Okada T, Haze K, Yanagi H, Yura T, Negishi M & Mori K. ATF6 activated by proteolysis binds in the presence of NF-Y (CBF) directly to the cis-acting element responsible for the mammalian unfolded protein response. *Molecular and Cellular Biology* 2000 **20** 6755–6767.
32 Kokame K, Kato H & Miyata T. Identification of ERSE-II, a new cis-acting element responsible for the ATF6-dependent mammalian unfolded protein response. *Journal of Biological Chemistry* 2001 **276** 9199–9205.

Received 24 January 2005
Accepted 7 April 2005

Available online at www.sciencedirect.com
SCIENCE DIRECT
Diabetes Research and Clinical Practice 70 (2005) 291–297
DIABETES RESEARCH AND CLINICAL PRACTICE
www.elsevier.com/locate/diabres

Secondary sulfonylurea failure: Comparison of period until insulin treatment between diabetic patients treated with gliclazide and glibenclamide☆

Jo Satoh [a,*], Kazuma Takahashi [a], Yumiko Takizawa [a], Hisamitsu Ishihara [a], Masashi Hirai [a], Hideki Katagiri [a], Yoshinori Hinokio [a], Susumu Suzuki [a], Ichiro Tsuji [b], Yoshitomo Oka [a]

[a] *Division of Molecular Metabolism and Diabetes, Department of Internal Medicine, Tohoku University Graduate School of Medicine, Sendai, Japan*
[b] *Department of Public Health, Tohoku University Graduate School of Medicine, Sendai, Japan*

Received 18 January 2005; received in revised form 15 April 2005; accepted 21 April 2005
Available online 8 June 2005

Abstract

We retrospectively evaluated a possible difference in periods until start of insulin treatment between type 2 diabetic patients treated with gliclazide (GCZ) and glibenclamide (GBC), because GCZ might be protective for beta cells than GBC. Subjects were Japanese patients. GCZ group consisted of patients treated with GCZ alone or with GCZ and GBC in the separate treatment periods in combination with or without other oral hypoglycemic agents (OHAs), while GBC group consisted of patients with GBC alone or in combination with other OHAs except GCZ. The periods until the treatment of insulin commenced were calculated using the Kaplan-Meier method. Proportional hazards models were used to adjust the differing variables between GCZ and GBC groups. The periods until the start of insulin treatment from diabetes onset, diabetes treatment, or GCZ or GBC treatment were significantly longer in the GCZ group than those in GBC group ($P < 0.001$ in each group). Independent variables affecting the period were average HbA1c levels during GCZ or GBC treatment (hazard ratio = 2.5 per %), other OHAs combined (hazard ratio = 1.9 on combination), and difference between GCZ and GBC groups (hazard ratio = 0.5 on GCZ). These results imply that GCZ may be more protective against secondary beta cell failure than GBC.

Keywords: Sulfonylurea; Sulfonylurea receptor; Beta cell; Secondary sulfonylurea failure; Gliclazide; Glibenclamide; Type 2 diabetes

1. Introduction

Insulin resistance and insulin deficiency are the major pathogenesis of type 2 diabetes and these factors co-exist to a various extent in each patient [1].

☆ This study was presented in the Meeting of the 18th International Diabetes Federation at Paris in 2003.

* Corresponding author. Present address: Department of Diabetes and Metabolism, Iwate Medical University, 19-1 Uchimaru, Morioka 020-8505, Japan. Tel.: +81 19 625 5083; fax: +81 19 625 5083.
E-mail address: jsatoh@iwate-med.ac.jp (J. Satoh).

0168-8227/$ – see front matter © 2005 Elsevier Ireland Ltd. All rights reserved.
doi:10.1016/j.diabres.2005.04.002

Blood glucose levels are usually well controlled by diet therapy and exercise in the early stage of type 2 diabetes. However, when control of blood glucose becomes poor, various hypoglycemic agents (OHAs) are used depending on the pathophysiology of each patient, e.g., α-glucosidase inhibitors for postprandial hyperglycemia, biguanides or thiazolidinediones for insulin resistance and nateglinide or sulfonylureas (SU) for deficiency of insulin secretion [2]. When insulin secretion is severely impaired and insulin secretagogues are ineffective, insulin therapy is required to control blood glucose levels even in the type 2 diabetes.

Among OHAs, SU is most commonly used worldwide for type 2 diabetes [3]. SU binds SU receptor of the beta cell and stimulates insulin secretion [4]. However, desensitization of insulin secretion with SU, known as secondary SU failure [5], sometimes occurs during the SU treatment. It is assumed that the SU failure is a state of secondary beta cell failure and that mechanisms of the secondary beta cell failure may include long-time over-stimulation of the beta cell with SU [6,7] and glucose toxicity [8], which could be induced by oxidative stress [9] and IL-1-β production of the beta cell under hyperglycemia [10]. Gliclazide (GCZ) and glibenclamide (GBC) are classes of SU used worldwide. Because GCZ is relatively weak insulin secretagogue [11,12] and has anti-oxidant [13–15] and anti-cytokine properties [16,17], GCZ might be more protective against secondary beta cell failure than GBC, which does not share the same characteristics as GCZ. To clinically reveal a different effect of GCZ and GBC on secondary beta cell failure, we retrospectively compared the periods until the commencement of insulin treatment from the onset of diabetes, from start of diabetes treatment, or from start of GBC or GCZ treatment.

2. Subjects and methods

2.1. Subjects

Subjects were Japanese patients with type 2 diabetes treated in our department from 1981 to 2000. All the subjects, who regularly (usually one a month) visited our department during 2000 and who had been treated with either GCZ or GBC since 1981 when GCZ was available in our department, were included in the study. GCZ group consisted of patients ($n = 106$) treated with GCZ alone or in combination with other OHAs [$n = 65$, administration period of GCZ was 4.6 ± 4.4 (mean ± S.D.) years and 2.9 (0.3–11.6) (median, 10–90 percentile) years], or patients treated with GCZ and GBC in the separate treatment periods, in combination with or without other OHAs [$n = 41$, administration period of GCZ was 4.2 ± 3.7 (mean ± S.D.) years and 4.2 (0.1–10.0) (median, 10–90 percentile) years, while that of GBC was 3.6 ± 3.4 (mean ± S.D.) years and 2.8 (0.1–9.0) (median, 10–90 percentile) years). In these 41 patients, GCZ was followed by GBC in 30 patients, white GBC was by GCZ in 11 patients. GBC group consisted of patients ($n = 168$) treated with GBC alone or in combination with other OHAs except GCZ [administration period of GBC was 4.4 ± 4.2 years (mean ± S.D.) and 3.0 (0.2–10.7) (median, 10–90 percentile) years]. Distribution of patient number was not different during 1981–2000 between GCZ group and GBC group.

2.2. Criteria for treatment with GCZ, GBC, or insulin

Doctors in charge determined a class and dosage of OHAs or insulin and the timing of when treatment commenced. When fasting plasma glucose and HbA1c levels were greater than approximately 140 mg/dl and 7%, respectively, even after dietary therapy and exercise had been performed for more than 3 months, a small dosage of GCZ (40 mg) or GBC (1.25 mg) began. However, when fasting plasma glucose and HbA1c levels were greater than approximately 170 mg/dl and 8%, respectively, even after the maximum dosage of GCZ (160 mg) or GBC (10 mg) had been used for more than 3 months, insulin therapy commenced. The maximum dosage was suggested in Japan by the Ministry of Health, Labour and Welfare of Japan. None of the patients were treated with a combination therapy of insulin and GCZ or GBC in those days.

2.3. Biochemical examinations

Blood glucose concentration and HbA1c were analyzed by a glucose analysis unit GA02U, A&T, and

by an auto-hemoglobin analysis HLC-723Ghbllls, Toso Co. (Tokyo, Japan), respectively.

2.4. Database

Various patient data including sex, birth date, age of onset of diabetes, BMI, fasting plasma glucose (FPG), HbA1c, and age of start of any OHAs (including GCZ and GBC), GCZ or GBC, or insulin, were serially recorded in an electronic chart, CoDic2000 (Novo Nordisc Pharma Co., Denmark).

2.5. Statistical analysis

The data in the CoDic2000 were transferred to Excel (Microsoft) and then statistically analyzed by unpaired *t*-test, Mann–Whitney test, or Chi-square test by Stat View-J5.0 (Abacus Concepts Inc., Berkeley, CA, USA). Periods until the start of insulin treatment were calculated using the Kaplan-Meier method (SPSS for Windows 11.0.1J, SPSS Co., Tokyo, Japan). Cox's Proportional hazard models were used to analyze independent variables affecting differences in the period between GCZ and GBC group.

3. Results

There was no significant differences between the two groups in background factors, such as sex, age, duration of diabetes, BMI, blood pressure, FPG levels and HbA1c at start of GCZ or GBC treatment, and combined OHAs or previous OHAs. However, FPG and HbA1c at start of any OHAs (including GCZ and GBC), and mean HbAfc until insulin treatment from start of any OHAs (including GCZ and GBC) and mean HbA1c until insulin treatment from start of GCZ or GBC treatment were significantly lower in GCZ group than that in GBC group (Table 1).

The periods until the start of insulin treatment was analyzed by the Kaplan-Meier method. The periods until the start of insulin treatment from diabetes onset, from start of any OHAs (including GCZ and GBC) treatment, and from start of GCZ or GBC treatment were significantly longer in GCZ group than those in GBC group ($P < 0.001$ in the each period, Logrank test) (Fig. 1) (Table 2). To adjust the differences in background factors between GCZ and GBC group and

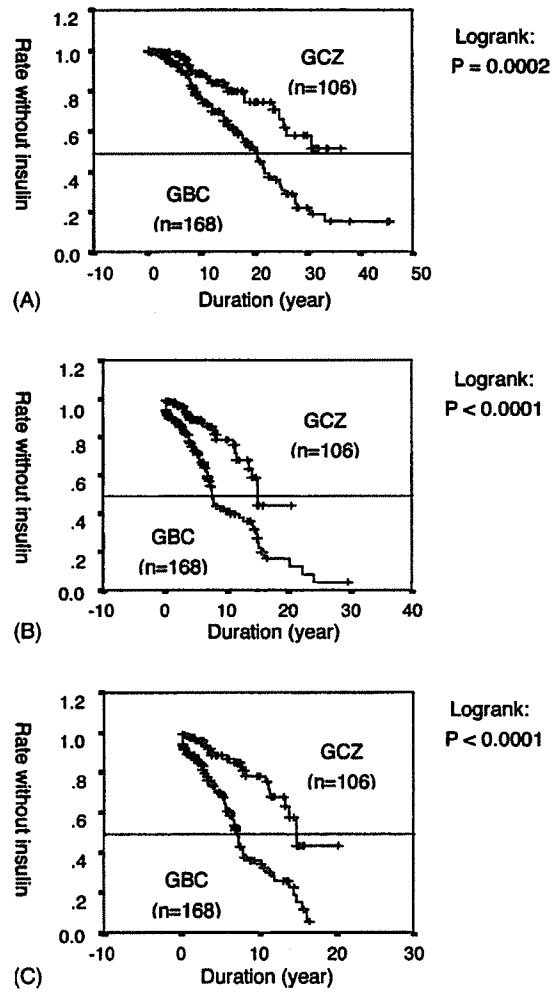

Fig. 1. The periods until start of insulin treatment from onset of diabetes (A), from start of any OHAs (including GCZ and GBC) (B) and from start of GCZ or GBC (C) were calculated by the Kaplan-Meier method.

to reveal the independent factors responsible for the different periods until state of insulin treatment between the two groups, Cox's proportional hazard model was used. Cox's proportional hazard analysis indicated that independent variables affecting the period were mean HbA1c (%) during GCZ or GBC treatment (hazard ratio = 2.5 per %, $P = 0.01$), other OHAs combined (hazard ratio = 1.9 on combination, $P < 0.01$), and difference between GCZ and GBG groups (hazard ratio = 0.5 on GCZ, $P = 0.01$) (Table 3A). Among various medicines used for combined therapy, hazard ratio (2.9) on thiazolidine-

Table 1
Characteristics of patients

Variables	GCZ (mean ± S.D.)	GBC (mean ± S.D.)	P
Number (male/female)	106 (60/46)	168 (81/87)	NS
Age (years)			
At onset of DM	48.9 ± 12.3	47.5 ± 13.5	NS
At start of any OHAs	56.0 ± 12.0	55.4 ± 14.4	NS
At start of GCZ or GBC	56.2 ± 11.9	56.2 ± 14.5	NS
Duration (years)			
Onset of DM—start of any OHAs	7.1 ± 7.0	7.8 ± 7.7	NS
Onset of DM—start of GCZ or GBC	7.3 ± 7.0	8.7 ± 8.2	NS
BMI (kg/m^2)	23.2 ± 3.4	23.9 ± 3.4	NS
Blood pressure (mmHg)			
Systolic BP	130.7 ± 13.2	131.0 ± 13.0	NS
Diastolic BP	77.0 ± 7.8	75.6 ± 6.9	NS
Fasting plasma glucose (mg/dl)			
At start of any OHAs	158.2 ± 41.7	169.6 ± 47.9	<0.05
At start of GCZ or GBC	163.4 ± 43.2	168.7 ± 45.5	NS
HbA1c (%)			
At start of any OHAs	7.3 ± 1.4	7.8 ± 1.6	<0.05
At start of GCZ or GBC	7.4 ± 1.4	7.7 ± 1.7	NS
Mean until insulin from start of any OHAs	6.8 ± 0.9	7.3 ± 1.2	<0.0001
Mean until insulin from start of GCZ or GBC	6.8 ± 0.9	7.4 ± 1.3	<0.0001
Combined OHAs (yes/no)	39/67	71/97	NS
Nateglinide	1	5	
Glimepiride	8	10	
Thiazolidinedione	6	13	
Biguanide	10	25	
Alpha-glucosidase inhibitor	30	57	
Other sulfonylureas	0	1	
Previous OHAs (yes/no)	89/17	140/28	NS

Table 2
Duration until start of insulin treatment

Duration until start of insulin (years)	GCZ (N = 106) (95% CI)	GBC (N = 168) (95% CI)	P
From onset of diabetes			
Mean	27.7 (24.7–30.7)	21.4 (18.7–24.2)	<0.001
Median	–	20.6 (17.7–23.5)	–
From start of any OHAs			
Mean	14.6 (12.7–16.5)	10.3 (8.5–12.0)	<0.001
Median	14.8 (13.5–16.2)	7.5 (6.8–8.2)	<0.0001
From start of GCZ or GBC			
Mean	14.5 (12.6–16.4)	8.0 (6.9–9.0)	<0.0001
Median	14.8 (13.4–16.2)	7.2 (6.4–8.0)	<0.0001

Table 3
Cox's proportional hazard analysis for change to insulin treatment

Variables	P	Hazard ratio
Part A		
Male sex	0.44	0.84
Age per year	–	0.92
At onset of diabetes	0.75	0.69
At start of any OHAs	0.98	1.12
At start of GCZ or GBC	0.91	1.13
Diabetes duration per year	–	0.96
From onset of diabetes to start of any OHAs	0.97	0.96
From onset of diabetes to start of GCZ or GBC	0.76	0.71
BMI per kg/m^2	0.82	1
Fasting plasma glucose per mg/dl		
At start of any OHAs	0.18	1
At start of GCZ or GBC	0.75	1
HbA1c per %		
At start of any OHAs	0.26	0.74
At start of GCZ or GBC	0.34	1.27
Mean until start of insulin from start of any OHAs	0.55	0.8
Mean until start of insulin from start of GCZ or GBC	0.01	2.51
On combined therapy	0.009	1.88
On previous therapy	0.62	1.39
On GCZ vs. GBC	0.01	0.47
Part B		
On combined therapy		
Nateglinide	0.48	0.46
Glimepiride	0.7	1.5
Thiazotidinedione	0.02	2.9
Biguanide	0.27	1.49
α-Glucosidase inhibitor	0.16	1.44
Other sulfonylureas	0.61	0.55

dione was significantly higher ($P = 0.02$) (Table 3B) by Cox's proportional hazard analysis.

4. Discussion

The period until the start of insulin treatment was significantly longer in type 2 diabetes patients treated with GCZ than those with GBC even after adjusting the different variables. These results imply that GCZ is more protective against secondary beta cell failure than GBC.

In the preliminary analysis, we compared the period until the start of insulin treatment among three groups. Group 1 ($n = 65$), patients treated with GCZ alone or GCZ combined with OHAs other than GBC. Group 2 ($n = 168$), patients treated with GBC alone or GBC combined with OHAs other than GCZ. Group 3 ($n = 41$), patients treated with GCZ and GBC in the separate treatment periods in combination with or without other OHAs. Among these three groups, the period until insulin treatment from the onset of diabetes is far longer ($P < 0.001$, Logrank) in Group 1 (mean = 33.3 years, median uncalculated) than that of the Group 2 (mean = 21.4 years, median = 20.6 years) or Group 3 (mean = 22.8 years, median 24.9 years) (data not shown). The significant time differences were also obtained in the period until insulin treatment from the start of any OHAs (including GCZ and GBC) and from the start of GCZ or GBC between Groups 1 and 2 or Group 3 (data not shown). However, there might be a bias in this preliminary analysis, because GCZ may have been preferably chosen to patients with lower, although not significant, FPG and HbA1c, whereas GBC with higher levels of FPG and HbA1c (data not shown), probably because physicians generally thought that GCZ was a less potent insulin secretagogue than GBC. Actually, GCZ was changed to GBC when GCZ was not effective in 30 out of 41 patients in Group 3, while GBC was changed to GCZ in 11 out of 41 patients. These preliminary data indicate that well-controlled patients with GCZ remained in Group 1, whereas poorly controlled patients with GCZ was moved to Group 3, and eventually resulted in insulin therapy.

To avoid this bias, we combined Groups 1 and 3 as the GCZ group, and compared the GCZ group with the GBC group (Group 2 in the preliminary analysis). As shown in Fig. 1 and Table 2, the periods until insulin therapy from any starting points, e.g., onset of diabetes, start of any OHAs (including GCZ and GBC) and start of GCZ of GBC, were still significantly longer in the GCZ group than those in the GBC group by the Kaplan-Meier analysis. Because the some background factors, such as FPG and HbA1c at start of any OHAs (including GCZ and GBC), and mean HbA1c during the treatments were different between the two groups (Table 1), the proportional hazard model was used to adjust the background factors and to analyze independent factors

affecting different prognosis between the two groups. As shown in Table 3A, the three independent factors were revealed, i.e., the mean HbA1c until start of insulin from start of GCZ or GBC, the combined therapy and the difference between the GCZ and GBC group.

The higher HbA1c until start of insulin from start of GCZ or GBC is an independent factor for starting insulin therapy (the odds ratio, 2.51 per 1% of HbA1c), indicating that the insulin therapy was preferably chosen to patients with poor glycemic control. It is interesting to note that the mean HbA1c levels during treatment with GCZ or GBC were significantly lower in the GCZ group than those in the GBC group, although HbA1c at the start of GCZ or GBC was not significantly different between the two groups (Table 1).

Another factor for earlier start of insulin treatment was the combined OHA therapy, although the percentage of patients with the combined therapy was not different between the GCZ and GBC group (Table 1). Among OHAs, the combination with the thiazolidinedione was an independent factor for starting insulin therapy (the odds ratio, 2.9 on thiazolidinedione) (Table 3B). It has been reported that the thiazolidinedione, an insulin sensitizer, has protective effects on the pancreatic islets [18]. This seems contradictory, but it could be interpreted that patients with poor glycemic control even with the maximum dosage of GCZ or GBC were preferably combined with the thiazolodinedione (troglitazone) in those days, but eventually received insulin therapy.

The third independent factor was the difference per se between GCZ and GBC group. Patients treated with GCZ less frequently received insulin treatment when compared with those treated with GBC (the odds ratio: 0.47 on GCZ). This implies that the secondary beta cell failure is less frequently observed with GCZ than with GBC. There are possible explanations for the protective effect of GCZ on the pancreatic beta cell, e.g., low affinity to SUR [11,12] and its anti-oxidant [13–15] and anti-cytokine properties [16,17].

GCZ and GBC bind sulfonylurea receptors (SUR). SURs consist of SUR1 (beta-cell type) and SUR2 (cardiac and smooth muscle types) [19,20]. SUR1 has an affinity to the residues of common sulfonylurea structure and benzamide, whereas SUR2 has an affinity to the benzamide residue [21]. It has been reported that GCZ has only the common residue of SU, whereas GBC has both the common SU residue and the benzamide residue [20]. Therefore, the potency and duration for insulin secretion is weaker and shorter, respectively, in GCZ compared with GBC [22], i.e., GCZ may not overstimulate and exhaust the beta cells as compared with GBC.

Another difference between GCZ and GBC is its anti-oxidant activity. It has been reported that GCZ, but not GBC, has a potent free radical-scavenging activity [13–15], which is mediated by the azabicyclo-octyl ring grafted on to its sulfonylurea core [13]. The oxidative stress increases under the chronic hyperglycemia, and a reduction of beta-cell mass and increased oxidative stress-related tissue damage that is correlated with the extent of the beta-cell lesions were shown in Japanese type 2 diabetic patients [23]. Recently, it has been reported that hyperglycemia-induced mitochondrial superoxide production activates the uncoupling of protein 2, decreases the ATP/ADP ratio and results in reducing glucose-stimulating insulin secretion [9]. Thus, the anti-oxidative activity of GCZ may protect the beta cells from oxidative stress-induced beta cell damage as recently reported [24].

Furthermore, it was suggested that hyperglycemia stimulates the beta cells to produce IL-1β, and IL-1β induces apoptosis of beta cells by an autocrine fashion [10]. We previously reported that GCZ, but not GBC, suppresses production of IL-1-β and TNF-α in vitro by human peripheral blood mononuclear cells and in vivo in mice [17]. This indicates that GCZ might also exhibit a protective effect on beta cells by suppression of IL-1-β.

In conclusion, the retrospective analysis has indicated that patients treated with GCZ needed to receive insulin treatment less frequently, and implies that GCZ is less likely to induce the beta cell failure including secondary SU failure as compared with GBC.

Acknowledgement

We thank Ms. Miwa Tsukamoto for inputting data to CoDiC2000.

References

[1] K.S. Polonsky, J. Sturis, G.I. Bell, Non-insulin-dependent diabetes mellitus: a genetically programmed failure of the beta cell to compensate for insulin resistance, N. Engl. J. Med. 334 (1996) 777–783.

[2] S.E. Inzucchi, Oral antihyperglycemic therapy for type 2 diabetes: scientific review, JAMA 287 (2002) 360–372.

[3] B.R. Zimmerman, Sulfonylureas, Endocrinol. Metab. Clin. North Am. 26 (1997) 511–522.

[4] N.C. Sturgess, M.L. Ashford, D.L. Cook, C.N. Hates, The sufphonylurea receptor may be an ATP-sensitive potassium channel. The sulphonyl urea receptor may be an ATP-sensitive potassium channel, Lancet 8453 (1985) 474–475.

[5] A.D. Harrower, Comparison of efficacy, secondary failure rate, and complications of sulfonylureas, J. Diabetes Complications 8 (1994) 201–203.

[6] S. Stenman, A. Melander, P.H. Groop, L.C. Groop, What is the benefit of increasing the sulfonylurea dose? Ann. Intern. Med. 118 (1993) 169–172.

[7] I. Rustenbeck, Desensitization of insulin secretion, Biochem. Pharmacol. 63 (2002) 1921–1935.

[8] H. Yki-Jarvinen, Glucose toxicity, Endocr. Rev. 13 (1992) 415–431.

[9] S. Krauss, C.Y. Zhang, L. Scorrano, L.T. Dalgaard, J. St-Pierre, S.T. Grey, et al. Superoxide-mediated activation of uncoupling protein 2 causes pancreatic beta cell dysfunction, J. Clin. Invest. 112 (2003) 1831–1842.

[10] K. Maedler, P. Sergeev, F. Ris, J. Oberholzer, H.I. Joller-Jemelka, G.A. Spinas, et al. Glucose-induced β cell production of IL-1β contributes to glucotoxicity in human pancreatic islets, J. Clin. Invest. 110 (2002) 851–860.

[11] K.J. Palmer, R.N. Brogden, Gliclazide. An update of its pharmacological properties and therapeutic efficacy in non-insulin-dependent diabetes mellitus, Drugs 46 (1993) 92–125.

[12] F. Gregorio, F. Ambrosi, S. Cristallini, M. Pedetti, P. Filipponi, F. Santeusanio, Therapeutical concentrations of tolbutamide, glibenclamide, gliclazide and gliquidone at different glucose levels: in vitro effects on pancreatic A- and B-cell function, Diabetes Res. Clin. Pract. 18 (1992) 197–206.

[13] Y. Noda, A. Mori, L. Packer, Gliclazide scavengers hydroxyl, superoxide and nitric oxide radicals. An ESR study, Res. Common Mot. Pathol. Pharmacol. 96 (1997) 115–124.

[14] R.C. O'Briens, M. Luo, The effects of gliclazide and other sulphonylureas on low-density lipoprotein oxidation in vitro, Metabolism 46 (Suppl.) (1997) 22–25.

[15] R.E. Jennings, N.A. Scott, A.R. Saniabadi, Effect of gliclazide on platelet reactivity and free radicals in type 2 diabetic patients: clinical assessment, Metabolism 41 (Suppl.) (1992) 36–39.

[16] A.-C. Desfaits, O. Serri, G. Renier, Normalization of plasma lipid peroxides, monocyte adhesion, and tumor necrosis factor-α production in NIDDM patients after gliclazide treatment, Diabetes Care 21 (1998) 487–493.

[17] M. Fukuzawa, J. Satoh, X. Qiang, S. Miyaguchi, Y. Sakata, T. Nakazawa, et al. Inhibition of tumor necrosis factor-alpha with anti-diabetic agents, Diabetes Res. Clin. Pract. 43 (1999) 147–154.

[18] D.S. Bell, Beta-cell rejuvenation with thiazolidinediones, Am. J. Med. 15 (Suppl. 8A) (2003) 20S–23S.

[19] F.M. Gribble, S.J. Tucker, S. Seino, F.M. Ashcroft, Tissue specificity of sulfonylureas: studies on cloned cardiac and beta-cell K(ATP) channels, Diabetes 47 (1998) 1412–1418.

[20] F.M. Ashcroft, F.M. Gribble, Tissue-specific effects of sulfonylureas: lessons from studies of cloned K(ATP) channels, J. Diabetes Complications 14 (2000) 192–196.

[21] J.C. Henquin, M.G. Garrino, M. Nenquin, Stimulation of insulin release by benzoic acid derivatives related to the non-sulphonylurea moiety of glibenclamide: structural requirements and cellular mechanisms, Eur. J. Pharmacol. 141 (1987) 243–251.

[22] P.S. van der Wal, R.J. Heine, Characteristics of pancreatic beta-cell secretion in type 2 diabetic patients treated with gliclazide and glibenclamide, Diabetes Res. Clin. Pract. 52 (2001) 103–111.

[23] H. Sakuraba, H. Mizukami, N. Yagihashi, R. Wada, C. Hanyu, S. Yagihashi, Reduced beta-cell mass and expression of oxidative stress-related DNA damage in the islet of Japanese type II diabetic patents, Diabetologia 45 (2002) 85–96.

[24] K. Kimoto, K. Suzuki, T. Kizaki, Y. Hitomi, H. Ishida, H. Katsuta, et al. Gliclazide protects pancreatic beta-cells from damage by hydrogen peroxide, Biochem. Biophys. Res. Commun. 303 (2003) 112–119.

THE JOURNAL OF BIOLOGICAL CHEMISTRY
Vol. 280, No. 16, Issue of May 6, pp. 18525–18535, 2005
Printed in U.S.A.

A Novel Protein Kinase B (PKB)/AKT-binding Protein Enhances PKB Kinase Activity and Regulates DNA Synthesis*

Received for publication, January 18, 2005
Published, JBC Papers in Press, March 7, 2005, DOI 10.1074/jbc.M500586200

Motonobu Anai‡, Nobuhiro Shojima§, Hideki Katagiri¶, Takehide Ogihara¶, Hideyuki Sakoda‡, Yukiko Onishi‡, Hiraku Ono‡, Midori Fujishiro§, Yasushi Fukushima§, Nanao Horike‖, Amelia Viana‖, Masatoshi Kikuchi‡, Noriko Noguchi, Shinichiro Takahashi‡‡, Kuniaki Takata§§, Yoshitomo Oka¶, Yasunobu Uchijima‖, Hiroki Kurihara‖, and Tomoichiro Asano¶¶**

*From the ‡Department of Internal Medicine, Institute for Adult Diseases, Asahi Life Foundation, 1-6-1, Marunouchi, Chiyoda-ku, Tokyo 100-0005, Japan, the ¶Division of Molecular Metabolism and Diabetes, Department of Internal Medicine, Tohoku University Graduate School of Medicine, 1-1 Seiryo-cho, Aoba-ku, Sendai, Miyagi 980-8574, Japan, the §§Department of Cell Biology, Institute for Cellular and Molecular Regulation, Gunma University, 3-39-15 Showamachi, Maebashi, Gunma 371-8512, Japan, and the §Department of Internal Medicine, Graduate School of Medicine, **Department of Molecular Biology and Medicine, Research Center for Advanced Science and Technology, ‡‡Department of Animal Sciences, Graduate School of Agriculture and Life Sciences, and ‖Department of Physiological Chemistry and Metabolism, Graduate School of Medicine, University of Tokyo, 7-3-1 Hongo, Bunkyo-ku, Tokyo 113-8655, Japan*

Protein kinase B (PKB)/Akt reportedly plays a role in the survival and/or proliferation of cells. We identified a novel protein, which binds to PKB, using a yeast two-hybrid screening system. This association was demonstrated not only *in vivo* by overexpressing both proteins or by coimmunoprecipitation of the endogenous proteins, but also *in vitro* using glutathione *S*-transferase fusion proteins. Importantly, this protein specifically associates with the C terminus of PKB but not with other AGC kinases and enhances PKB phosphorylation and kinase activation without growth factor stimulation. Thus, we termed this Akt-specific binding protein APE (Akt-phosphorylation enhancer). Since APE-induced phosphorylation of PKB did not occur in cells treated with wortmannin or LY294002, APE itself is not a kinase but seems to enhance or prolong the phosphoinositide 3-kinase-dependent phosphorylation of PKB. In cells in which APE was suppressed by small interfering RNA, DNA synthesis was significantly reduced with suppression of PKB phosphorylation, suggesting a synergistic role of APE in PKB-induced proliferation. On the other hand, in cells overexpressing both PKB and APE, despite markedly increased basal phosphorylation of PKB, both DNA rereplication and subsequent Chk2 phosphorylation and apoptosis were seen, suggesting the involvement of APE in the regulation of cell cycling replication licensing. Taking these observations together, APE appears to be a novel regulator of PKB phosphorylation. Furthermore, the interaction between APE and PKB, possibly dependent on the expression levels of both proteins, may be a novel molecular mechanism leading to proliferation and/or apoptosis.

The serine/threonine protein kinase PKB[1] (also called Akt) is thought to be a key mediator of signal transduction. Upon growth factor stimulation, a family of lipid kinases known as class 1 phosphoinositide 3-kinases (PI 3-kinases) is recruited to the plasma membrane. PI 3-kinases phosphorylate phosphatidylinositol 4,5-bisphosphate at the D-3 position of the inositol ring, converting it to phosphatidylinositol 3,4,5-trisphosphate. Following the activation of PI 3-kinase, PKBs are recruited to the plasma membrane through direct contact of the pleckstrin homology (PH) domain with phosphatidylinositol 3,4,5-trisphosphate and are phosphorylated at Thr^{308} by PDK1 and at Ser^{473} by PDK2, a kinase of which the molecular structure has not yet been identified (1, 2). AGC kinases other than PKB are also known to be regulated by PI 3-kinase, and PKB acts downstream from PI 3-kinase to regulate numerous biological processes, such as proliferation, antiapoptosis, cell growth, and glucose metabolism (1, 2).

PKB has a wide range of substrates, including GSK-3, FKHR (FoxO1), FKHR-L1 (FoxO3), AFX (FoxO4), and eNOS, all of which have the consensus motif RXRXX(S/T) (3, 4). Protein kinases do not generally form stable complexes with their substrates, although PKB has been shown to exist in a stable complex with several of its substrates including MDM2, $p21^{Cip1}$/WAF1, and TSC2 (5–8). It was recently shown that several proteins interact with PKB as function modulators rather than as substrates. In a specific subset of T and B cells, TCL1 interacts with the PH domain of PKB and increases its kinase activity (9). Heat shock protein 90 (Hsp90) was shown to form complexes with Cdc37 and PKB, and PKB was stabilized and protected from dephosphorylation and degradation, resulting in increased kinase activity (10). Carboxyl-terminal modulator protein binds to the carboxyl terminus of PKBα. Carboxyl-terminal modulator protein binding reportedly inhibits the phosphorylation and kinase activity of PKB, and stable expression of carboxyl-terminal modulator protein leads to phenotypic regression of

* This work was supported in part by a grant from Takeda Science Foundation. The costs of publication of this article were defrayed in part by the payment of page charges. This article must therefore be hereby marked "*advertisement*" in accordance with 18 U.S.C. Section 1734 solely to indicate this fact.

¶¶ To whom correspondence should be addressed: Dept. of Physiological Chemistry and Metabolism, Graduate School of Medicine, University of Tokyo, 7-3-1 Hongo, Bunkyo-ku, Tokyo 113-8655, Japan. Tel.: 81-3-5841-3603; Fax: 81-3-5803-1874; E-mail: asano-tky@umin.ac.jp.

[1] The abbreviations used are: PKB, protein kinase B; PI, phosphoinositide; PH, pleckstrin homology; GST, glutathione *S*-transferase; PARP, poly(ADP-ribose) polymerase; MTT, 3-[4,5-Dimethylthiazol-2-yl]-2,5-diphenyltetrazolium bromide; GFP, green fluorescent protein; siRNA, small interfering RNA; BrdUrd, bromodeoxyuridine; PKC, protein kinase C.

a v-Akt transformed lung epithelial cell line to wild type (11). TRB3 was also identified as a negative modulator of the PKB type (12), although a contradictory report was very recently published (13). These results indicate that understanding PKB modulation is important for elucidating the mechanism of PKB activation and its regulation of cellular functions.

In this study, we identified a novel protein that interacts with PKB (*in vivo* and *in vitro*). Without growth factor stimulation, overexpression of this protein markedly enhances phosphorylation of Thr^{308} and Ser^{473} in PKB, leading to its kinase activation and phosphorylation of its downstream substrates such as GSK-3 and FKHR. In addition, suppression of APE using RNA interference significantly reduces PKB phosphorylation and PKB kinase activity. Therefore, we termed this protein APE (Akt-phosphorylation enhancer) and herein demonstrate the possible role of APE in DNA synthesis and apoptosis in cooperation with PKB.

MATERIALS AND METHODS

Yeast Two-hybrid System—The DupLEX-A two-hybrid system (OriGene) was used for screening. We screened a mouse embryonic cDNA library with the pJG4-5 vector with a bait protein corresponding to the full length of mouse PKBα using a pEG202 vector and yeast strain EGY48. The positive clones were selected and assayed for β-galactosidase activity. Plasmid DNAs were isolated from positive clones and co-transformed with bait cDNA or negative control cDNA back into yeast to reconfirm the interaction. A yeast β-galactosidase assay kit (Pierce) was used to measure the protein-protein *in vivo* interaction according to the manufacturer's instructions.

Northern Blotting—Mouse Multiple Tissue Northern blot (Clontech) was used for Northern blotting. APE cDNA corresponding to the 600 bp of the coding region of the C-terminal and 400 bp of the untranslated region was used as a probe.

Antibody against APE—Fragments of the cDNA clone were subcloned into a glutathione *S*-transferase (GST) expression vector (Amersham Biosciences), expressed in BL21 and purified using glutathione-coupled Sepharose beads. Purified GST fusion proteins were injected into rabbits, and antisera were affinity-purified using the respective antigens. APE-C was generated to a fragment of APE encompassing amino acids 1646–1845. APE-N1 corresponded to amino acids 172–372, and APE-N3 to corresponded to 501–601. Polyclonal antibodies to each antigen were affinity-purified, using each GST fusion protein, after removal of GST-specific antibody.

Gene Constructions and Expression System in Yeast and Mammalian Cells—Full-length APE cDNAs were cloned into the pShuttle vector to express these proteins with an adenovirus expression system (Clontech). The expression cassette was excited and subcloned into pAdeno-X vector (Clontech). Adenovirus was cloned, and large scale virus purification from 293T cell lysates was achieved by performing CsCl density gradient centrifugation twice, followed by overnight dialysis as previously described. An adenovirus expression vector for PKBα with a Myc tag at its C terminus had previously been generated (14). PKBβ, the PKBα PH domain (residues 1–106), the PKBα kinase domain (residues 138–418), PKBα kinase and its hydrophobic domain (residues 148–480), and the PKBα hydrophobic domain (residues 418–480) were generated by PCR using PKBα or PKCβ cDNA as described previously (14). SGK1 (residues 98–431), SGK2 (residues 35–333), PKCβ2 (residues 342–673), and PKCε (residues 408–737) were generated by PCR using a mouse testis cDNA template. APE fragments were generated by PCR using full-length cDNAs as templates. The PCR products were cloned into pEG202 or pJG4-5 vectors.

Cell Cultures—HepG2, COS-7, and HeLa cells were from the RIKEN Cell Bank. Cells were maintained in Dulbecco's modified Eagle's medium supplemented with 10% fetal bovine serum under a 5% CO_2 atmosphere at 37 °C.

Immunoblot Analysis—The antibodies used in this study were anti-Myc (Upstate Biotechnology), anti-Akt, anti-phospho-Thr^{308}-Akt, anti-phospho-Ser^{473}-Akt, anti-phospho-Thr^{68}-Chk2, anti-phospho-Ser^{256}-FKHR, anti-phospho-$Ser^{20/9}$-GSK-3α/β, anti-caspase 3, anti-cleaved caspase 3, anti-poly(ADP-ribose) polymerase (PARP), anti-cleaved PARP (Cell Signaling Technology) anti-FLAG and anti-α tubulin (Sigma). For total cell lysates, cells were washed with ice-cold phosphate-buffered saline twice and collected with Laemmli sample buffer containing 100 mM dithiothreitol before separation by SDS-10% to 6% or 10% polyacrylamide gel. Proteins were transferred to nitrocellulose membranes. Immunoblotting was performed with ECL according to the manufacturer's instructions.

In Vivo Association of APE and PKB—HeLa cells were resuspended (4×10^7 cells/ml) in buffer A (10 mM HEPES (pH 7.9), 10 mM KCl, 1.5 mM $MgCl_2$, 0.34 M sucrose, 10% glycerol, 1 mM dithiothreitol, 5 μg/ml aprotinin, 5 μg/ml leupeptin, 0.5 μg/ml pepstatin A, 0.1 mM phenylmethylsulfonyl fluoride). Mouse testis was homogenized with 50 strokes, using a Teflon/glass homogenizer, in 10 volumes of ice-cold buffer A. Triton X-100 (0.1%) was added, and the cells were incubated for 5 min on ice. The supernatant was clarified by high speed centrifugation (15 min, 20,000 × *g*, 4 °C) to remove nuclei, cell debris, and insoluble aggregates. Endogenous PKB and APE in the HeLa cell lysate or mouse testis lysates were immunoprecipitated with 100 μg of immobilized anti-PKB and anti-APE-C antibodies, respectively. One hundred micrograms of immobilized Rabbit IgG were used as a control. The immunoprecipitates were washed four times in buffer A with 0.1% Triton X-100, eluted with elution buffer, electrophoresed, and transferred to nitrocellulose membranes. These filters were subjected to inmmunoblotting using the antibodies against APE and PKB.

In Vitro Association of APE and PKB—cDNAs encoding amino acids 418–480 of mouse PKBα with the Myc tag and amino acids 1646–1845 of mouse APE with the FLAG tag at their C termini were amplified by PCR. These cDNAs were cloned into pGEX-5X-1 and pET-28a vectors, and fusion protein expressions were induced in *E. coli* strain BL21 by the addition of 0.1 mM isopropyl β-D-thiogalactoside. The expressed proteins were purified using GST or His tag, according to the manufacturer's instructions. GST alone, GST-APE fragment fusion protein, and GST-PKB fragment fusion protein were incubated with glutathione-Sepharose 4B beads (Amersham Biosciences) for 3 h at 4 °C followed by extensive washing in NETN buffer (20 mM Tris-HCl, pH 8.0, 100 mM NaCl, 1 mM EDTA, 0.5% Nonidet P-40). An aliquot containing 20 μg of GST alone and GST-APE fragment fusion protein bound to beads were then incubated with the His tag PKB fragment. Similarly, an aliquot containing 20 μg of GST alone and the GST-PKB fragment fusion protein bound to beads were then incubated with the His tag APE fragment. After a 4-h incubation at 4 °C, the beads were washed five times with NETN buffer. The bound proteins were eluted by incubating the beads in SDS loading buffer containing 0.1 M dithiothreitol, electrophoresed, and then immunoblotted using anti-Myc and anti-FLAG antibodies for detection of the His tag PKB fragment and His tag APE fragment, respectively.

Immunoprecipitation and PKB Kinase Assay—Cells were lysed in Nonidet P-40 lysis buffer (50 mM Tris-HCl pH 7.5, 1% Nonidet P-40, 120 mM NaCl, 1 mM EDTA, 50 mM NaF, 40 mM β-glycerophosphate, 0.1 mM Na_3VO_4, 1 mM phenylmethylsulfonyl fluoride, 10 μg/ml aprotinin, 50 μg/ml leupeptin). For co-immunoprecipitation, we incubated protein lysates with primary antibodies overnight at 4 °C followed by incubation with Protein A-Sepharose. Immunoprecipitates were washed three times with Nonidet P-40 lysis buffer. An Akt kinase assay kit (Cell Signaling Technology) was used to measure PKB kinase activity. PKB was immunoprecipitated with anti-Myc antibody and Protein G-Sepharose. PKB kinase activity was detected using GSK-3β recombinant protein as a substrate according to the manufacturer's instructions.

Gene Transduction and in Vivo Phosphorylation of PKB—Mammalian cell lines were infected with adenovirus the day after plating. Purified virus was added directly to the culture medium. Titers of adenovirus for protein overexpression were adjusted so that the expression levels of the Myc-tagged PKBα were similar, irrespective of APE co-expression. Likewise, APE expression levels were adjusted so as to be similar, irrespective of Myc-tagged PKBα co-expression. Experiments were performed 36 h later for *in vivo* phosphorylation. Cells were starved for 12 h with KRB-Hepes buffer (118.5 mM NaCl, 4.7 mM KCl, 2.5 mM $CaCl_2$, 1.2 mM KH_2PO_4, 1.2 mM $MgSO_4$, 24.9 mM $NaHCO_3$, 30 mM HEPES, pH 7.4) containing 20 mg/ml bovine serum albumin. Cells were stimulated by the indicated stimulant in each experiment and, whenever indicated, 1 μM wortmannin or 10 μM LY294002 1 h prior to stimulation.

Gene Silencing by siRNA—Gene silencing was performed by an adenovirus-mediated siRNA method. For silencing of endogenous APE gene expression in HepG2 cells, a sense fragment (GGATCCGCATTAACACCCACCCGCTCTTCAAGAGAGAGCGGGTGGGTGTTAATGTTTTTTTCTAGAGAATTC) and an antisense fragment (GAATTCTCTAGAAAAAACATTAACACCCACCCGCTCTCTCTTGAAGAGCGGGTGGGTGTTAATGCGGATCC) were used for human APE. These two oligonucleotides were annealed *in vitro*, and the resultant double-stranded DNA fragments were subcloned into the BamHI-EcoRI site of a pSIREN-Shuttle vector. A negative control vector was supplied by Clontech. The expression cassette containing siRNA of APE or the negative control was excited and subcloned into pAdeno-X vector.

A

```
   1  MENEIFTPLLEQFMFSPLVTWVKTFGFLAAGNGTNLDEYVALVDGVFLNQVMLQINPKSE
  61  SQRVNKKVNNDASLRIHNLSILVKQIKFYQETLQQLIMMPLPDILIIGKNPFSRQGTEE
 121  VKKLLLLLLGCAVQCQKKEEFIEKIQGLDFDTKAAVAAHIQEVTHNQENVFDLQVMEVTD
 181  MSQEDIEPLLKNMVSHLERLIDERDEHSETIVELSEERDGVHFLPHASSSAQSPCGSPGM
 241  KRTESRQNLSVELADAKAKIERRLRQELEEKTEQLLDCKQELEQIEVELKRLQQENMNLLS
 301  DARSARMYRDELDALREKAVRVDKLESELSRYKERLHDIEFYKARVRELKEDNQVLLETK
 361  TMLEDQLEGTPAREDKLHELEKENLQLKAKLHDMEMEPDMDRKKIEELMEENMTLEMAQK
 421  QSMDESLHLGNELEQISRTSELAEAPQKSLGHEVNELTSSKLLKLEMENQSLTKTVEELR
 481  STADSAAGSTSKILEVEKENQRLNKKVETLENEIIQEKQSLQNCQNLSKDLMKEKAQLEK
 541  TIETLRENSERQIKILEQENERLNQTVSSLRQRSQISAEARVKDIEKENKILHESIKETC
 601  GKLSKIEFEKRQMKKSLELYKEKGEPASELENELNHLGKENELLQKKITNLKETCEKLST
 661  LEQENSELEPENRKFKKTLDSFKNLTFQLESLEKENSQLDEENLELRRSVESLKCASMRM
 721  AQLQLENKELESEKEQLPKGLEIMRASFKKTERLEVSYQGLETENQRLQKALENSNKKTQ
 781  QLESELQDLEMENQTLQKSLEELKISSKRLEQLEKENKSLEQETSQLEKDKAQLEKENKR
 841  LRQQAEIKDETLEENNVKIGNLENENKTLFKEINVYKESCVRLKELEKENKELVSRATED
 901  IKTLVTLPEDLVSEKLKTQQMNNDLEKLTHELEKIGLNKERLLHDEQSTDDSRYKLLESK
 961  LESTLKKSLEIKEEKIAALEARLEESTNYNQQLRHELKTVKKNYEALKQRQDEERMVQSS
1021  IPVEGEDDKWGEESQEATRELLKVKDRLIEVERNNATLQAEKQALKTQLKQLETQNNNLQ
1081  AQILALQRQTVSLQEQNTTLQTQNAKLQVENSTLNSQSTSLMNQNAQLLIQQQSSLENEN
1141  SIMKEREDLKSLYDALIKDHEKLELLHERQASEYESLISKNGTLKSAHKNLEVEHKDLED
1201  RYNQLLKQKGQLEDLESMIKTEQEKMLESKNHEVVASEYKKLQGENDRLNYTYSQLLKE
1261  TEILQMDHKNLKSVLNNSKLEQTRLEAEFSKLKEQYQQLDETSTKLNNQCELLSQLKGNL
1321  EEENRHLLDQIQTLMLQNRTLLEQNMESKDLFHVEQRQYIDKLNELRRQKELEEKIMDQ
1381  YKFYDPSPERRRGNWITLKMRKLISKKDDLNFEPQKSLTLTPTRSDSSEGFLQLPNQDSQ
1441  DSSSVGSNSLEDGQTLGTKKSSTMNDLVQSMVLAGGQMTGSTENLEVPDDISTGSRRKEL
1501  GAMAFSTTATNFSTVNSSAAFRSKQLVNNKDTTSFEDISPQGISDDSSTGSRVHASRPAS
1561  LDSGMTSISNSNNNASLHEVKAGAVNTQSRPQSHSSGDESELLHDHETWSSSGSSPIQYLK
1621  RQTRSSPMLQNKISETIESRAHHKMKAGSPGSEVVTLQQFLERSNKLTSIQLKSSSQENL
1681  LDEVMKSLSVSSDFLGKDKPVSCTLARSVSGKTPGDFYDRNTTKPEFLFTGPQKTEDAYT
1741  ISSAGKPTFSTQGKIKLVKETSVSRQSKDSNPYATLERAISVISTAEGTTRRTSIHDFLS
1801  KDSRLPVSVDSSPPTAGSSSTTASNVNKVQESRNSKSRSPEQQSS
```

B

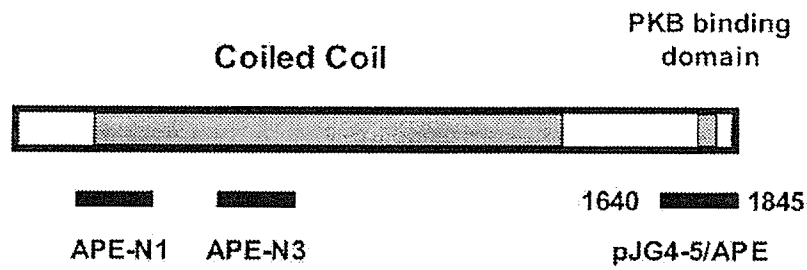

FIG. 1. **Structure and sequence of APE.** *A*, amino acid sequence of mouse APE. *B*, cDNA clones of APE isolated from the yeast two-hybrid screen and the fragments (APE-N1, APE-N3, and APE-C identical to pJG4–5/APE) used to generate an APE-specific antibody are shown *aligned below* a representation of full-length APE.

DNA Synthesis—HepG2 cells were maintained in Dulbecco's modified Eagle's medium supplemented with 10% fetal calf serum for 36 h and then transfected with an adenovirus encoding siRNA of APE or the negative control. Seventy-two hours after transfection, culture media were changed to Dulbecco's modified Eagle's medium supplemented with 0.2% bovine serum albumin, and cells were incubated for an additional 24 h. The cells were then incubated with BrdUrd labeling solution for 4 h. Incorporated BrdUrd was detected by cell proliferation ELISA, BrdUrd (colorimetric) (Roche Applied Science).

3-[4,5-Dimethylthiazol-2-yl]-2,5-diphenyltetrazolium Bromide (MTT) Assay—Cellular proliferation was measured by reduction of MTT, which corresponds to the living cell number and metabolic activity (15). Cells were plated at 5×10^4 cells/well in 24-well plates and transfected with adenovirus. After incubation for the indicated time, MTT solution was added to each well. After 1 h of incubation, the reaction was stopped by adding 1 ml of isopropyl alcohol with 0.04 N HCl. The absorbance of each well was measured at 492 and 630 nm using a microplate reader.

Cell Viability Analysis—HepG2 cells and HeLa cells were infected with control GFP, PKB, APE, or both PKB and APE adenoviruses and incubated for the indicated times. Floating cells were recovered from culture medium by centrifugation at $1200 \times g$ for 1 min, and adherent cells were harvested by trypsinization. Both the floating and adherent cells were observed for morphologic changes with a light microscope at ×200 magnification. We combined the adherent and floating cells and measured their viability by using a trypan blue dye exclusion assay.

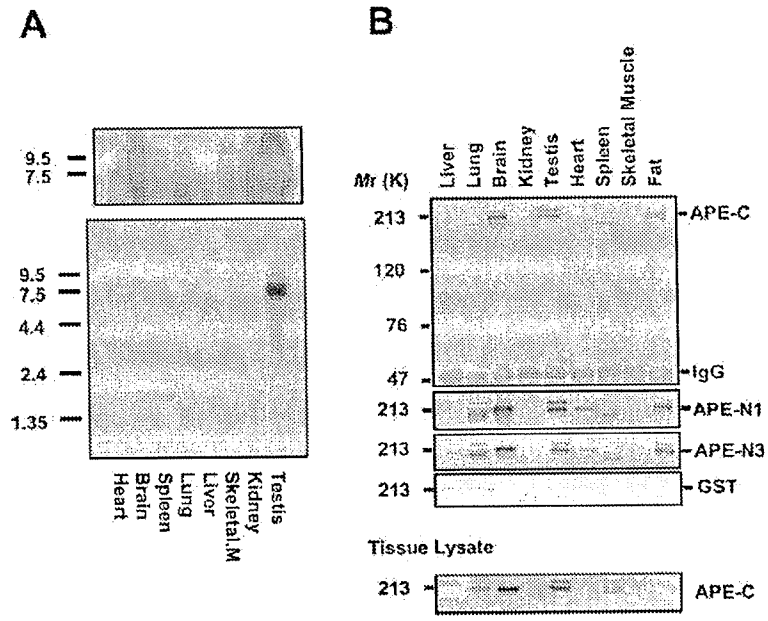

FIG. 2. **Tissue distribution of APE.** *A*, multiple tissue Northern (*MTN*; Clontech) blots probed with 3′ coding and untranslated region of APE. The *upper panel* represents the results of long exposure. *B*, Western analysis of APE. 50 μg of each tissue protein were immunoprecipitated with α-APE-C and immunoblotted with α-APE-C, α-APE-N1, α-APE-N3, and α-GST (*first* to *fourth panels*). Lysates of mouse tissues without immunoprecipitation were also used for immunoblotting with α-APE-C (*bottom panel*). The portions recognized by each antibody are shown under "Materials and Methods" and in Fig. 1.

Cell Cycle Analysis by Flow Cytometry—For cell cycle synchronization, cells were arrested at the G_1-S phase transition separated by two subsequent thymidine blocks (2 mM thymidine) for 14 h, separated by a period of 10 h without thymidine. Both adherent and nonadherent cells were harvested by trypsinization, and an aliquot of 2×10^6 cells was fixed in ice-cold ethanol for at least 1 h at 4 °C. The cells were collected by centrifugation and resuspended in propidium iodine (10 μg/ml) solution containing RNase for analysis of DNA content. Data were then collected on a BD Biosciences FACScan, 20,000 events/sample, using Cellquest software. DNA content analysis was performed with Verity ModFit software for the Macintosh computer.

RESULTS

Cloning of cDNAs Encoding the Protein Binding with PKB—Using full-length mouse PKB as bait in a yeast two-hybrid screen of an embryonic mouse complementary DNA library, we isolated 31 clones displaying β-galactosidase activity. Sequencing analysis revealed 10 of the clones with the strongest β-galactosidase activity to be identical. In all cases, 606 bp of the coding region were followed by a 3′-untranslated region. Isolation of the full-length cDNA by phage screening of the mouse embryonic cDNA library and a series of 5′ rapid amplifications of cDNA ends by PCR showed the largest open reading frame to be 5538 bp, which encode a 1845-amino acid protein with a predicted relative molecular mass (M_r) of 212,478 (Fig. 1*A*, accession number AB087827). By searching several data bases, we found that some mouse clones (BC037020, BC079895, AK129310) and this cDNA to be identical to a mouse homologue of the Kazusa DNA Research Institute clone KIAA1212. This clone is located on mouse chromosome 11 and on human chromosome 2. Although some cDNAs in the data base are presented as "full-length," it seems that they are not, judging from the size of the protein shown in this study. Our mouse cDNA is very likely to be full-length, and this protein was subsequently shown to enhance the phosphorylation of PKB, such that we designated the clone APE (Akt-phosphorylation enhancer). Protein analysis of APE revealed it to be a hydrophilic protein, and that its N terminus has a significant similarity with the putative coiled coil domain of the myosin heavy chain (Fig. 1*B*).

Tissue Distribution of APE—Northern blot analysis detected a 7.9-kb band of APE messenger RNA in the testis (Fig. 2*A*). Longer exposure revealed moderate expression in the brain, and low expressions in the spleen and lungs (Fig. 2*A*, *upper panel*). Anti-APE antibodies were generated against the three different portions of APE (Fig. 1*B*). Immunoblotting with antibodies against APE, irrespective of the differences in the

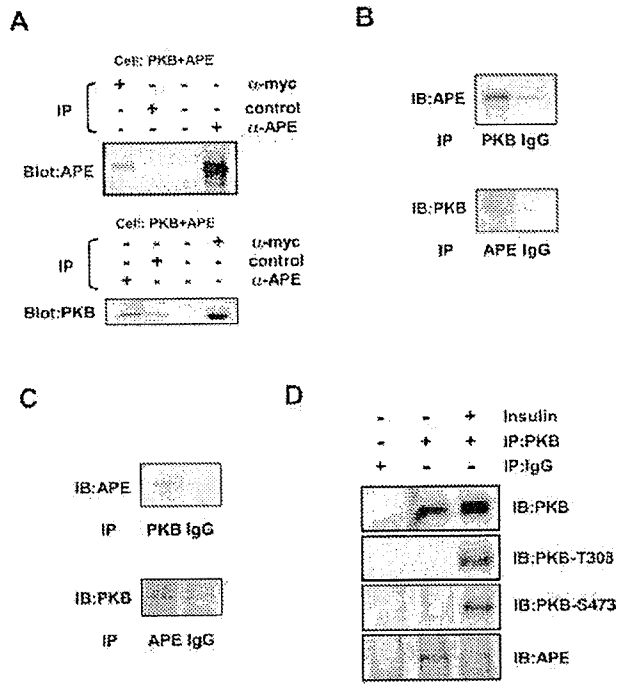

FIG. 3. **Interactions of APE with PKB *in vivo*.** *A*, binding of APE to Myc-PKB. Both APE and Myc-PKB were expressed in COS-7 cells. Immunoprecipitations (*IP*) from cell lysates were performed with the antibodies indicated on the *upper side* of *A*. Immunoblotting (*IB*) using anti-APE-C (*upper panel*) or anti-PKB (*lower panel*) is shown. APE was co-immunoprecipitated with PKB. Endogenous APE and PKB bind *in vivo*. HeLa cells (*B*) or mouse testes (*C*) were homogenized and immunoprecipitated with the antibody indicated *below* the *panels*. APE specifically immunoprecipitated with anti-PKB antibody, and PKB specifically immunoprecipitated with APE antibody. *D*, interaction of APE and PKB was inhibited after insulin stimulation. HEK293 cells were serum starved for 24 h and treated with 100 nM insulin for 15 min. Endogenous PKB were immunoprecipitated with α-PKB monoclonal antibody or with control IgG, and the amount of APE associated with PKB was analyzed by Western blotting.

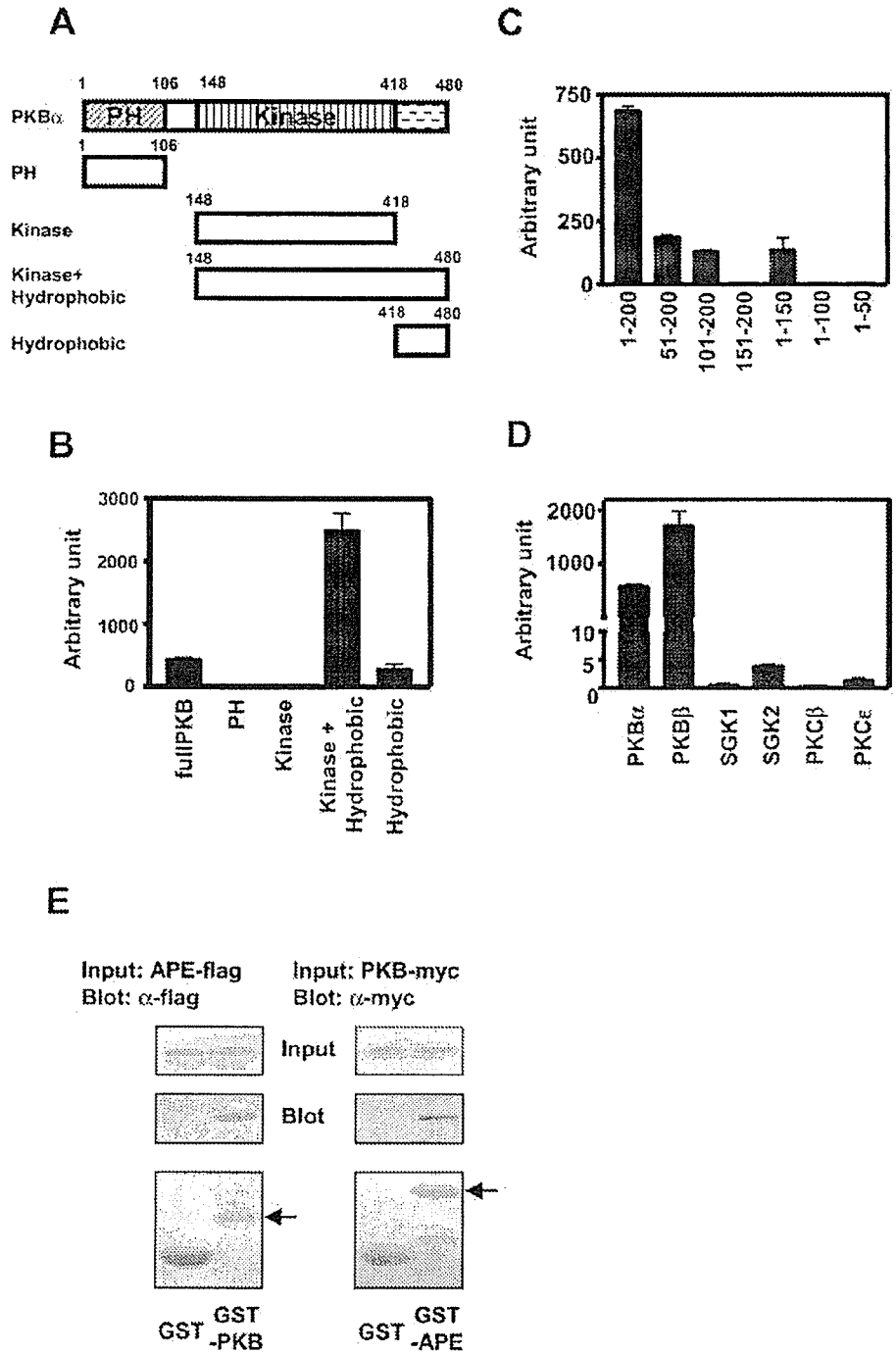

FIG. 4. **APE is a PKB-specific binding protein and has a domain responsible for the association.** *A*, PKBα structural domains and pEG202-PKBα fusion proteins. *B*, *in vivo* interaction of APE and PKBα structural domain. Interactions of APE-200 amino acids with PKBα, the PH domain, kinase domain, kinase domain with the hydrophobic domain, and the hydrophobic domain of PKBα are indicated as arbitrary units. *C*, *in vivo* interactions of PKBα and APE fragments. pEG202-PKBα was expressed in EGY48 with the indicated portion of the C-terminal of APE. β-Galactosidase activity is indicated as arbitrary units. *D*, *in vivo* interactions of APE and AGC kinases. pEG202-PKBα was expressed in EGY48 with PKBα, PKBβ, SGK1, SGK2, PKCβ, or PKCε. These *in vivo* interactions were measured by β-galactosidase activity. *E*, physical association of APE and PKB *in vitro*. Extracts from *E. coli* BL21 cells expressing PKBα or APE with a pET system were used to test for APE or PKBα binding to the following bead matrices: GST beads coupled to either bacterially expressed GST or GST-PKB (amino acids 418–480) or GST-APE (amino acids 1646–1845). Extract bead complexes were washed three times to remove weakly bound protein prior to eluting off specifically bound proteins. The pulled down APE (FLAG-tagged) and PKBα (Myc-tagged) were resolved on an SDS-polyacrylamide gel and detected by α-FLAG or α-Myc antibody.

epitopes of these antibodies (Fig. 1*B*), identified three bands of 220, 213, and 203 kDa in mouse tissues, whereas the control antibody against GST did not recognize any of these bands (Fig. 2*B*). The largest band of 220 kDa was observed in the lungs, testis, and fat. The 213-kDa band was detected in the brain, testis, heart, and fat. Finally, the smallest (203-kDa) band was detected in the lungs and spleen. These results were similarly obtained by immunoblotting of either immunoprecipitates of

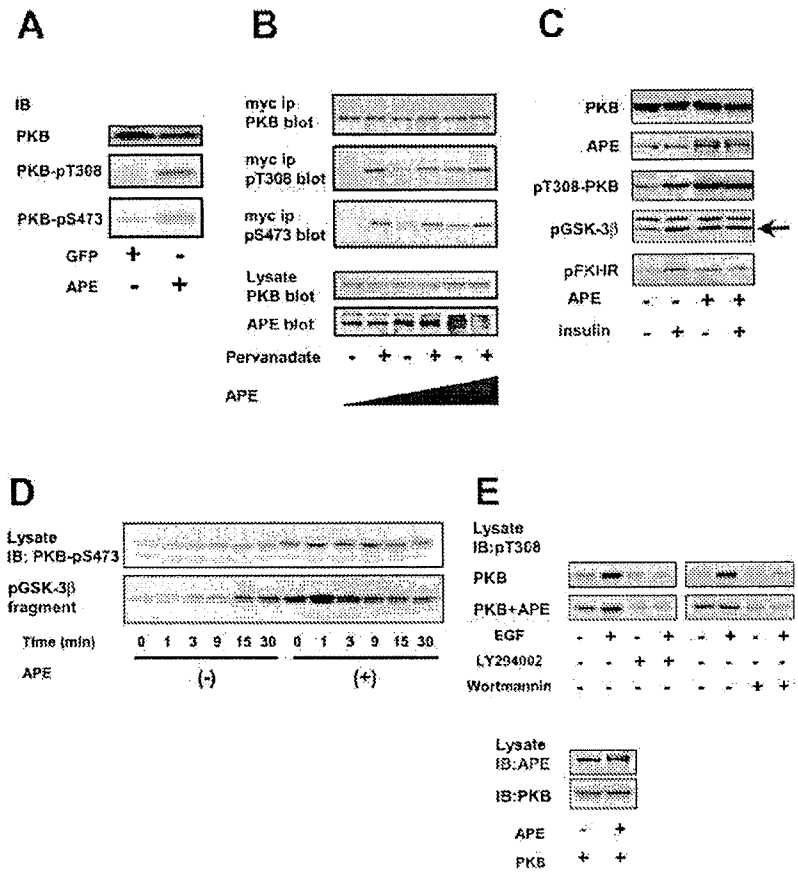

FIG. 5. **APE enhances basal PKB activity without growth factor stimulation.** *A*, basal phosphorylation of native PKB was enhanced by APE. COS-7 cells were transfected with GFP or APE and then serum-starved for 12 h. Basal phosphorylations of Thr^{308} and Ser^{473} were detected by specific antibodies. *IB*, immunoblot. *B*, APE enhances basal PKB phosphorylation without pervanadate stimulation. COS-7 cells were co-transfected with Myc-PKBα and with increasing amounts of APE. Cells were next serum-starved for 12 h and then stimulated with vehicle or 100 μM pervandate for 15 min at 37 °C. Cell lysates were next immunoprecipitated with Myc antibody, and the phosphorylation states of Thr^{308} and Ser^{473} were determined by specific antibodies. *C*, APE enhances downstream PKBα without insulin stimulation. HepG2 cells were transfected with Myc-PKBα and with or without APE, as indicated in *C*. Cells were serum-starved for 12 h and then stimulated with 10^{-7} M insulin for 15 min. Phosphorylations of Ser^{9} of GSK-3β and Ser^{256} of FKHR were detected by specific antibodies. *D*, APE enhanced PKB kinase activity without pervanadate stimulation. Myc-PKBα was transfected into COS-7 cells in the presence or absence of APE, as indicated. Cells were serum-starved and then stimulated with vehicle control or 100 μM pervanadate for the indicated times. Myc-PKB was immunoprecipitated, and phosphorylation of Ser^{473} of PKB was detected by a specific antibody. An *in vitro* kinase assay was performed using a GSK-3β fragment as the substrate for PKB kinase, and kinase activity was determined using the GSK-3β phospho-Ser^{9} antibody. *E*, APE-induced basal phosphorylation of PKBα was inhibited by LY294002 and wortmannin. COS-7 cells were transfected with Myc-PKBα, with or without APE. Cells were serum-starved for 12 h and then stimulated with 50 μM epidermal growth factor for 15 min. The cells were incubated with 10 μM LY294002 or 1 μM wortmannin for 1 h prior to epidermal growth factor stimulation.

tissue lysates (Fig. 2*B*, *upper panel*) or nonimmunoprecipitated lysate (Fig. 2*B*, *lower panel*). These results suggest the existence of alternatively spliced protein products from the APE gene because a search of human expressed sequence tag databases indicated the existence of alternatively spliced forms of APE (data not shown).

In Vivo Association of PKB and APE—Next, to demonstrate *in vivo* association between APE and PKB, full-length APE and c-Myc-tagged PKBα were overexpressed in COS-7 cells. As shown in the *upper panel* of Fig. 3*A*, APE was detected in the immunoprecipitate by the anti-Myc antibody (Fig. 3*A*, *upper panel*). Similarly, PKB was detected in the anti-APE immunoprecipitate (Fig. 3*A*, *lower panel*). This interaction between APE and PKB was demonstrated when both were overexpressed in Sf-9 insect cells or HepG2 cells (data not shown).

We also demonstrated an endogenous interaction between PKB and APE by coimmunoprecipitation of the endogenous proteins using specific antibodies in HeLa cells, and mouse testis. As shown in Fig. 3*B*, APE was coimmunoprecipitated by anti-PKB antibody in HeLa cells. PKB was also coimmunoprecipitated by anti-APE-C antibody as shown in the *lower panel*. The PKB and APE interaction was reconfirmed by the same procedure using mouse testis homogenates (Fig. 3*C*), indicating that the PKB-APE interaction occurs under physiological conditions.

APE Binds to Nonphosphorylated PKB More Efficiently than Phosphorylated PKB—The effect of PKB phosphorylation on the interaction between APE and PKB was assessed by measuring the amount of APE co-immunoprecipitated with PKB in the presence and absence of insulin stimulation (Fig. 3*D*). Insulin stimulation induced the phosphorylation of PKB on Thr^{308} and Ser^{473}. The amount of APE co-immunoprecipitated with PKB was revealed to be significantly lower in the insulin-stimulated condition, compared with the unstimulated condition (Fig. 3*D*, *bottom panel*). This result suggests that APE has a higher affinity for nonphosphorylated than for phosphorylated PKB.

APE Binds to the C-terminal Portion of PKB but Not to Other AGC Kinases—To determine the region of PKB responsible for binding with APE, we generated four deletion mutants consist-

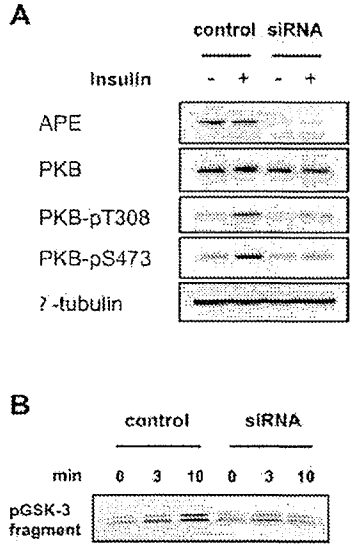

FIG. 6. **APE siRNA reduced insulin-stimulated endogenous PKB phosphorylation and kinase activity in HepG2 cells.** HepG2 cells were transfected with adenovirus expressing negative control siRNA or APE siRNA for 60 h, starved for 12 h, and treated with 100 nM insulin for 15 min. *A*, endogenous PKB were immunoprecipitated with α-PKB monoclonal antibody, and PKB phosphorylation was analyzed by Western blotting using phosphospecific antibodies of Thr^{308} or Ser^{473}. PKB and APE expression levels were analyzed using cell extracts. *B*, endogenous PKB immunoprecipitated by α-PKB monoclonal antibody from control or APE-depleted HepG2 cells was also used for an *in vitro* kinase assay.

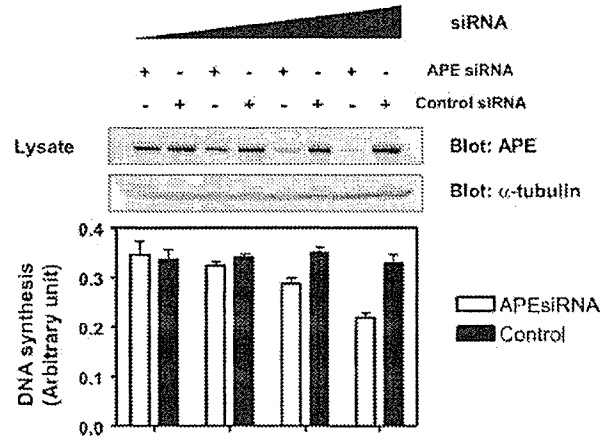

FIG. 7. **Phosphorylation of PKB and DNA synthesis were reduced by knockdown of APE.** HepG2 cells were transfected with adenovirus expressing negative control siRNA or APE siRNA. DNA synthesis in cells cultured in Dulbecco's modified Eagle's medium supplemented with 0.2% bovine serum albumin was measured by BrdUrd incorporation.

ing of a PH domain, kinase domain, kinase and hydrophobic domain, or the hydrophobic domain in the carboxyl terminus of PKB (16) (Fig. 4*A*). These mutants were subjected to baits in a yeast two hybrid screening with APE. It was revealed that the kinase domain with the hydrophobic motif or the hydrophobic motif alone binds with APE, whereas neither PH nor the kinase domain can bind with APE (Fig. 4*B*).

Subsequently, several deletion mutants of APE were produced to determine the portion responsible for the association with PKB. The C-terminal portion was shown to consist of 200 amino acids of APE, sufficient for the association with PKB. Since the deletion mutant amino acids 101–200 or 1–150 retain the ability to bind PKB, it is likely that the minimal portion necessary for the association with PKB is located within amino acid sequence 101–150 (Fig. 4*C*).

PKB belongs to a family of protein kinases, originally including protein kinase A, cGMP-dependent protein kinase and protein kinase C, termed the AGC family. Proteins in this family contain regions of high homology in their kinase domains (1). Since AGC kinases contain regions of high homology with the hydrophobic motif in PKB, we further examined whether APE interacted with AGC kinases other than PKB, using a yeast two-hybrid system. SGK1, SGK2, PKCβ2, PKCε, and PKBβ/Akt2 have a kinase domain and a hydrophobic motif highly homologous to those of PKBα. As a result, PKBβ and PKBα bind efficiently to APE in yeast (Fig. 4*D*). Conversely, very little interaction with APE was observed for SGK1, SGK2, PKCβ2, or PKCε. These results indicate that APE is not a common AGC kinase-binding protein but, rather, a PKB-specific binding protein.

In Vitro Association between Amino Acids 418–480 of PKB and Amino Acids 1646–1845 of APE—To examine whether the association of APE and PKB occurs *in vitro*, amino acids 418–480 of PKB and 1646–1845 of APE were expressed using *E. coli* and then purified. As shown in the *left panel* of Fig. 4*E*, GST-amino acids 418–480 of mouse PKBα fusion protein bound to His-tagged amino acids 1646–1845 of mouse APE protein, whereas GST alone did not. Similarly, GST-amino acids 1646–1845 of mouse APE fusion protein, but not GST alone, bound to His-tagged amino acids 418–480 of mouse PKBα (Fig. 4*E*, *right panel*). These results indicate that the interaction between APE and PKB is direct.

APE Markedly Enhances Basal Phosphorylation of PKB—PKBα is activated via phosphorylation of Thr^{308} in the activation loop of the kinase domain and of Ser^{473} in the hydrophobic motif of the carboxyl terminus (17–21). To test the effect of APE binding on phosphorylation of PKB, basal phosphorylation of endogenous PKBα in COS-7 cells transfected with GFP adenovirus or APE adenovirus was analyzed. As shown in Fig. 5*A*, there was no significant phosphorylation on Thr^{308} or Ser^{473} of PKBα after 12-h serum starvation (*left lane* of Fig. 5*A*), but Thr^{308} and Ser^{473} of endogenous PKB were apparently phosphorylated in cells overexpressing APE. A similar result was obtained for HepG2 cells (data not shown).

Pretreatment with pervanadate increased PKB phosphorylation, time-dependently, as reported previously (11). To explore the effect of APE on enhanced PKBα phosphorylation, we treated COS-7 cells with adenoviruses expressing PKBα and various amounts of APE. APE overexpression increased PKB phosphorylation, in a titer-dependent manner, and the maximal phosphorylation of PKB obtained by APE overexpression was comparable with that achieved by long term pervanadate stimulation (Fig. 5*B*). These results suggest that APE overexpression can induce essentially maximal phosphorylation of PKB on Thr^{308} and Ser^{473}, which indicates that APE is an enhancer of PKB *in vivo*.

Phosphorylation of PKB by APE Induces the Phosphorylation of GSK-3α/β and FKHR—PKB reportedly phosphorylates several downstream molecules such as GSK-3α/β and FKHR (17, 22). As a positive control, we confirmed that insulin stimulation induced PKB phsphorylation as well as downstream phosphorylation of Ser^{256} of FKHR and Ser^{9} of GSK-3β in HepG2 cells. Then we examined whether PKB phosphorylated by the overexpressed APE can induce the phosphorylations of GSK-3β and FKHR without growth factor stimulation. As shown in the right two lanes of Fig. 5*C*, overexpressed APE markedly enhanced phosphorylation of Ser^{256} of FKHR and Ser^{9} of GSK-3β, to degrees similar to those seen with insulin stimulation.

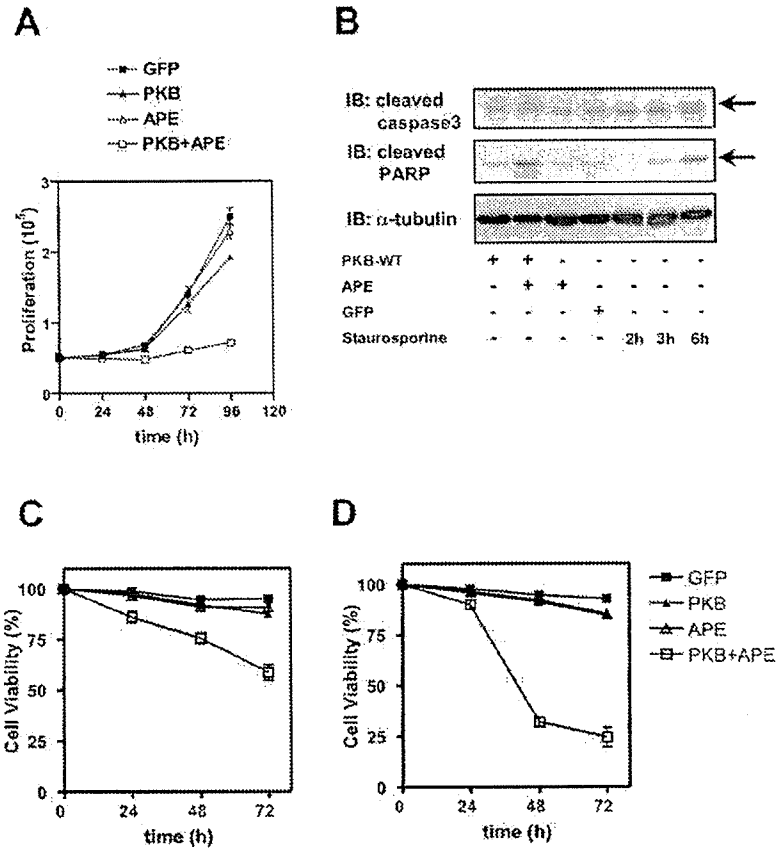

FIG. 8. **Inhibition of cell proliferation and induction of apoptosis by APE.** *A*, overexpressions of PKB and APE inhibited cell growth. COS-7 cells were transfected with adenoviruses encoding GFP, PKBα, APE, or PKBα with APE. At the indicated time after transfection, MTT assays were performed to measure cell growth. *B*, PKB and APE induce caspase-3 and PARP cleavage. COS-7 cells were either uninfected or infected with adenoviruses encoding GFP, PKBα, APE, or PKBα plus APE, for 36 h. The uninfected cells were treated with 500 ng/ml staurosporine for the indicated time prior to harvest. Cells were lysed and separated by SDS-PAGE and Western blotted (*IB*) with the indicated antibodies, shown on the *left*. *C* and *D*, overexpression of PKB and APE reduced cell viability. COS-7 cells (*C*) and HepG2 cells (*D*) were transfected with adenovirus encoding GFP, PKBα, APE, and PKBα with APE. Cell viability was measured by trypan blue dye exclusion assay.

In Vitro Kinase Activity of PKB Enhanced by APE—To test the influence of APE binding on PKB kinase activity, we assayed kinase activity in immune complexes from transfected COS-7 cells treated with pervanadate. Pervanadate-stimulated PKB activity was time-dependently increased when COS-7 cells were transfected with PKB alone, and kinase activity paralleled the phosphorylations of Thr^{308} and Ser^{473}. APE enhanced the basal phosphorylations of Thr^{308} and Ser^{473}, and *in vitro* kinase activity was also maximally enhanced and paralleled these phosphorylations. These results indicate that APE induces maximal basal phosphorylation of PKB, thereby maximally enhancing its kinase activity (Fig. 5*D*).

PI 3-Kinase Activity Is Needed for APE-induced PKB Phosphorylation—To examine whether the APE-induced increase in PKB phosphorylation is mediated only by PI 3-kinase, we examined the effects of the PI 3-kinase specific inhibitors LY294002 and wortmannin on APE-induced PKB phosphorylation. As shown in Fig. 5*E*, both epidermal growth factor-induced and APE-induced phosphorylation of PKB were completely inhibited by LY294002 and wortmannin treatments. These results indicate PI 3-kinase activity to be essential for APE-induced phosphorylation of PKB.

APE siRNA Inhibits Insulin-stimulated PKB Phosphorylation and Activation—To verify the role of endogenous APE in PKB phosphorylation, HepG2 cells were transfected with the negative control or small interfering RNA (siRNA) mediated by the adenoviral expression system. Suppression of endogenous APE by APE siRNA overexpression markedly reduced the APE protein level (Fig. 6*A*, *upper panel*). Under these conditions, endogenous PKB phosphorylation of both Thr^{308} and Ser^{473} in response to insulin was apparently reduced (Fig. 6*A*, *third* and *fourth panels*). Consistent with the PKB phosphorylation results, insulin-induced PKB kinase activity measured by *in vivo* kinase assay was also reduced in APE-deficient cells (Fig. 6*B*).

Knockdown of APE Reduces DNA Synthesis—To explore the effect of APE depletion on proliferation, DNA synthesis in HepG2 cells were measured by BrdUrd incorporation. It was shown that suppressed expression of endogenous APE by siRNA led to decreased DNA synthesis in an APE siRNA titer-dependent manner (Fig. 7).

Cell Death Induced by Overexpression of Both APE and PKB—Recent investigations have shown that overexpression of constitutively activated PKB mutants in many cell types promotes cellular proliferation and inhibits apoptosis (23–25). On the contrary, several lines of evidence indicate that down-regulation of PI 3-kinase/PKB is required to execute the mitotic program efficiently (26). To explore the effect of prolonged PKB activation induced by APE, we next analyzed the effect of APE on cellular proliferation using COS-7 cells (Fig. 8*A*). The expression of GFP protein by adenovirus had no effect on COS-7 proliferation. COS-7 cells expressing PKBα proliferated slightly more slowly than the control GFP-expressing cells. However, COS-7 cells expressing both PKBα and APE showed essentially no proliferation. Trypan blue exclusion was employed to assay cell viability in COS-7 cells and HepG2 cells overexpressing PKB and APE. COS-7 cells expressing both PKBα and APE showed reduced viability (*i.e.* these cells ultimately died) (Fig. 8*C*). Virtually the same observations were made in HepG2 cells (Fig. 8*D*).

Induction of Apoptosis by Overexpression of Both APE and PKB—To elucidate whether apoptosis is involved in the molecular mechanism of APE-induced inhibition of cellular proliferation and cell death, we analyzed the cleavage of caspase-3 and PARP (Fig. 8*B*). Caspase-3 and PARP are key mediators of apoptosis, and cleavage of these enzymes to their active form correlates with the onset of apoptosis (27, 28). When COS-7